Hybrid Optimisation Studies on the Microstructural Properties and Wear Resistance of Maraging steel 1.2709 Parts Produced by Laser Powder Bed Fusion

Divine Kudakwashe Maodzeka[1,2,3a]; Eyitayo Olatunde Olakanmi[1,2,3b]; Mosalagae. Mosalagae[1,2,3c*]; Devon. Hagedorn-Hansen[4,d]; Sisa Lesley Pityana[5,e].

[1] *Department of Mechanical, Energy & Industrial Engineering, Botswana International University of Science & Technology (BIUST), Palapye, Botswana.*

[2] *UNESCO Chair in Advanced Manufacturing (UCAM) Team, Botswana International University of Science & Technology, Palapye, Botswana.*

[3] *Advanced Manufacturing & Engineering Education (AMEE) Research Group, Botswana International University of Science & Technology, Palapye, Botswana.*

[4] *Department of Industrial Engineering, Stellenbosch University, Stellenbosch, South Africa.*

[5] *Laser Enabled Manufacturing (LEM) Research Group, National Laser Centre, Council for Scientific & Industrial Research (CSIR), Pretoria, South Africa.*

[a] md19100070@studentmail.biust.ac.bw

[b] olakanmie@biust.ac.bw

[*c] *Corresponding author:* mosalagaem@biust.ac.bw

[d] devonh@sun.ac.za

[e] SPityana@csir.co.za

Abstract

Improper selection of laser powder bed fusion (LPBF) process parameters tends to result in poor quality parts which imposes limitations with respect to the mechanical performance due to process induced defects. To address this LPBF processing challenge, this study employs a hybrid optimisation technique which combines artificial neural network (ANN) and response surface methodology (RSM) models. The models were employed for predicting the microstructural properties (porosity, microhardness and amount of martensite phase composition) and mechanical characteristic (wear resistance) of LPBF manufactured maraging steel 1.2709 parts as a function of a combination of process parameters (scan speed, laser power and hatch spacing). Both ANN and RSM models had a high tracking ability. However, ANN showed better prediction accuracy

than RSM. The most desirable optimum LPBF processing parameters for minimum wear volume and porosity while maintaining maximum microhardness and martensite phase composition were found at volumetric energy density (VED) of 77 J/mm³ (laser power = 165 W, scan speed = 784 mm/s and hatch spacing = 91 μm). Optimum quality properties predicted by the RSM and ANN models were consistent with confirmatory experiment results.

Keywords: Maraging steel 1.2709, Laser Powder Bed Fusion (LPBF), Artificial Neural Network (ANN), Response Surface Methodology (RSM), Wear Resistance.

1.0 Introduction

Laser powder bed fusion (LPBF) is an additive manufacturing (AM) technology. It allows the building of useful three-dimensional (3D) parts directly from a computer aided design (CAD) model. Consecutive layers of metal powder particles are melted and solidified on top of each other by the energy of an elevated intensity laser beam [1]. It is economically and technically efficient because of the basic principle of adding material based on a 3D CAD model, layer after layer, without a need for fixtures or tools. The complex 3D CAD model is reduced into simple two-dimensional slices. Quantity has a limited impact on manufacturing cost and lead time because there is no need for individual tooling or CAM programming, since LPBF is a CAD driven process [2]. Other advantages of LPBF include versatility in processing a wide range of materials, production of near net shape parts that are ready to use, increased functionality, and the ability to set the quality properties of products during processing by varying process parameters and scanning strategies. However, certain applications of LPBF fabricated parts are hindered by poor surface finish as well as dimensional and geometrical inaccuracies when compared to conventionally machined parts. LPBF fabricated part quality can also be compromised by various process induced defects, which includes porosity as a result of insufficient fusion and gas entrapment [3].

Materials that can be processed using LPBF include alloys of iron, nickel, titanium, copper, cobalt [4] and alloys of aluminium [5]. In this study maraging steel (DIN 1.2709) powder was used. Maraging steels are a class of iron-based alloys mainly consisting of alloying elements such as nickel, cobalt, molybdenum and titanium. The elements are added to produce intermetallic precipitates. The precipitated particles hinder the movement of dislocations thereby strengthening

the steel [6]. Typical applications for maraging steels include missile and rocket motor cases, drill chucks, extrusion tooling, punching tools, metal casting dies, plastic injection moulds, high performance shafting, gears, and fasteners [7]. Maraging steels are particularly suitable for the LPBF manufacturing process because of their good weldability and their relative ease to transform the austenite to a martensitic structure.

Mechanical and microstructural properties of parts produced by LPBF process are mainly determined by the materials and process parameters as well as post processing heat treatment conditions they are subjected to. Poor product quality may result from improper combination of process parameters [8]. Hence it is imperative to investigate the effect of LPBF process parameters on the resulting microstructure and mechanical properties of LPBF fabricated maraging steel. The most significant parameters on mechanical and microstructural properties are laser power and scanning speed [9]. The focal point of this study is on the effect of laser power, scan speed and hatch spacing with a view of optimising the LPBF process parameters for minimum wear volume. However, the impact of the process parameters on microstructural properties (porosity, microhardness and phase composition) cannot be ignored. Hence, these microstructural quality characteristics are investigated and their inter-relationship with the wear resistance of LPBF fabricated samples is established.

Several studies have investigated the mechanical and microstructural properties of maraging steel. Guo and Sha, [10] designed an ANN model for predicting the mechanical properties of maraging steel parts in relationship to process parameters, working temperature, and alloy composition. Their study focused on ageing temperature, ageing time, and deformation degree. The quality properties they studied were mechanical properties (including fracture toughness, ultimate tensile strength, hardness, elongation and impact energy) and martensitic conversion start temperature. The study concluded that desired maraging steel properties can be attained by applying the ANN model. Yasa et al., [7] assessed the effect of scan speed and layer thickness at constant laser power of approximately 105W on quality properties. Influence of laser re-melting and heat treatment were also investigated. Island scanning strategy was utilised to mitigate the impact of thermal gradients and thermal induced stresses. The investigated quality properties included micro and macro hardness, surface quality, relative density, toughness and tensile strength of maraging steel 1.2709 parts produced by LPBF. The outcome of their study revealed that energy density have

significant influence on relative density of the maraging steel parts. In the tested range of scan speed was found to have significant impact on the relative density. Layer thickness and scan speed was observed to have insignificant effect on microhardness. High hardness was obtained at 480^{o}C aging temperature and 5 hours aging time. The study inferred that the samples produced by LPBF achieved higher hardness and strength than conventionally manufactured samples. Mutua et al., [8] applied a full factorial experimental design to optimize processing parameters and post heat treatment processes on microstructure and mechanical properties of LPBF manufactured maraging steel. Process parameters investigated by their study were laser power, scan speed, pitch, spot diameter, solution and aging treatment as well as quality properties (surface morphology, microstructure, hardness and densification behaviour). Samples were built on Matsuura LUMEX Avance-25 hybrid machine. Laser power was varied from 100-400W, scan speed from 400-1000mm/s, pitch from 0.025-0.2 mm and spot diameter varied 0.05-0.3mm. Established optimum process conditions on that specific machine were scan speed 700mm/s, overlap rate of 40%, laser power of 300W and energy density of 71.43J/mm^3. The study observed higher hardness and strength on parts manufactured by LPBF than on conventionally produced parts, a similar observation was found by [7]. Much work has been done on the influence of LPBF processing parameters on mechanical properties such as fracture toughness, hardness and tensile strength. However, very general and little work was done on wear behaviour of LPBF fabricated maraging steel [11]. Optimum processing parameters on the microstructural properties (porosity, microhardness and phase composition) and wear resistance of LPBF manufactured maraging steel still remain unclear. Ahmed *et al*., [13] defined wear as, "a process in which material gets removed from either or both sliding elements under the influence of prime variables namely speed, load and sliding distance". Applications of maraging steel are limited by their relatively low hardness (HRC 50-57) and low wear resistance. For example they cannot be used for manufacturing cutting tools because of their lower hardness [14]. Some studies reported that tribological applications of any material can be improved by its wear properties [13].

The employment of a hybrid of RSM and ANN modelling has gathered a developing interest in engineering and other various fields of study [15], [16], [17], [18], [19], [20]. Rezaei *et al.*, [16] used ANN and RSM to optimise nanofiber diameter. The study compared ability of RSM and ANN models to optimise. It was concluded that both models results were in harmony with experimental data. However RSM predictions had better accuracy than ANN predictions. A study

conducted by Sada, [19] on modelling performance of ANN and RSM in predicting tensile strength of a welded part inferred that ANN had better prediction ability than RSM. According to Sada, [19] predictive abilities of RSM and ANN on non-linear relationships may differ due to the difference in their interpolation and extrapolation capabilities. Hence it is necessary to perform comparative analysis of their capabilities.

Guo and Sha, [10] defined ANN modelling as, "a non-linear statistical analysis technique which is essentially a black box linking input data to output data using a particular set of non-linear functions". ANN uses examples of a target function to determine the coefficients that make a certain mapping function estimate the target function as closely as attainable. ANN models does not require a long list of physics based equations. They automatically learn the correlation between the input data and output targets based on previous data. Neural networks map properties of phenomenon presented to it by detecting relationships of the presented data during its training phase and updates itself. Advantages of neural networks are that they make it possible to forecast investigated phenomenon of an arbitrary set of the input data. They do not require statistical and mathematical models of the investigated phenomenon [21]. Artificial neural networks have the capability to learn from their environment. This is useful when complexity of the data makes it difficult and almost impractical [22].

Response surface methodology (RSM) is a collection of statistical, graphical and mathematical methods that are useful to develop, improve and optimize processes [23]. The objective of RSM is to optimize a response (output variable) which is influenced by various independent (input) variables. RSM is superior to ANN because of its ability to explain the relationship between input variables and their response using of main effects plots. The interaction of the parameters can be visualized by the contour and surface plots [15]. In this study, a hybrid of ANN and RSM was employed to optimise the microstructural properties (microhardness, porosity and amount of martensite phase composition) and wear volume. A hybrid of response surface methodology and artificial neural network was employed to utilize the advantages of the two optimisation methods.

The main objectives of this study were to:

a. Develop RSM and ANN model which predicts mechanical properties of LPBF fabricated maraging steel 1.2709 samples.

b. Investigate the influence of LPBF process parameters on microstructural features (porosity, microhardness and martensite phase) and wear resistance of maraging steel 1.2709 parts.
c. Establish the relationship between the microstructural properties and wear resistance of LPBF fabricated maraging steel with a view to optimising its quality characteristics.
d. Compare RSM and ANN models predictions to define the best approach.
e. Establish optimum LPBF processing parameters for depositing defect-free layers of maraging steel 1.2709 via hybrid optimization technique which combines ANN and RSM.

2.0 Experimental Design and Analysis

A hybrid optimization methodology of RSM and ANN that was employed in this study to optimise the microstructural properties and wear resistance of maraging steel is summarized in Figure 1 [17], [18].

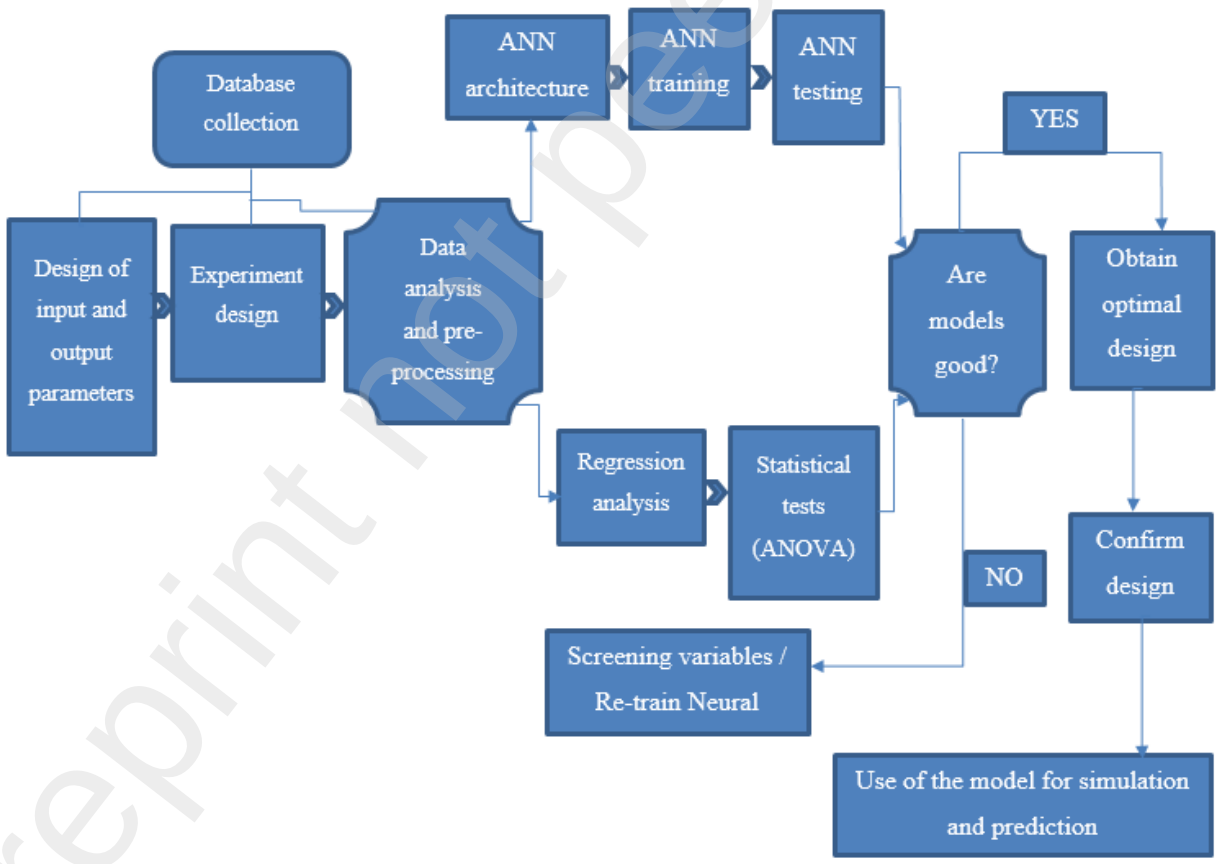

Figure 1 Procedure for implementing hybrid optimisation of the microstructural properties and wear resistance of LPBF fabricated maraging steel samples

Database collection was the first step in the hybrid optimisation methodology (Table 5). Data obtained from a set of experiments was used to develop a RSM model and train a developed ANN architecture. Both models were used to obtain optimum responses.

2.1 Response surface modelling (RSM) technique

A central composite design (CCD), a subcategory of response surface methodology in Minitab 17 software, was used to obtain experimental data for exploring the influence of LPBF processing parameters (Table 4) on the microstructural characteristics and wear resistance of LPBF fabricated maraging steel (1.2709) samples. Laser power, hatch spacing and scan speed were the three process independent variables considered with layer thickness being kept at constant 30 μm. The three variables were varied at three levels, they were ranked high alpha level, high level, zero level, low level and low alpha level (Table 1). Two star points were used for each variable.

Table 1

Selected process variables

Parameters	Laser power [W]	Scan speed [mm/s]	Hatch spacing [μm]
Designations	A	B	C
High alpha level (1.6818)	186.82	784	103.4
High level (1)	180	750	100
Zero level (0)	170	700	95
Low level (-1)	160	650	90
Low alpha level (-1.6818)	153.18	616	86.6
Variation range	20	100	10

In CCD, 6 central experimental points and 14 axial points making up 20 runs of experiments were engaged to optimise the microstructural characteristics and wear volume of LPBF fabricated maraging steel 1.2709 samples as process parameters were altered.

A quantitative pattern of relationship between responses y that depends on the controllable independent variables $x_1,x_2,x_3,\ldots\ldots x_k$ which was used to evaluate the responses in RSM can be generalized by equation 1 [18].

$$\boldsymbol{y = f(x_1,x_2,x_3,\ldots\ldots x_4) \pm \varepsilon} \quad (1)$$

Where the nature of the true response function f is not known, usually f is a first order or second order polynomial. ε is the error in the system, that is, other sources of variability not accounted for

in f. For example, effects such as background noise, effect of other variables, and measurement error on the response [24].

A response surface that consist of linear, square, and cross product terms approximation by utilising the fitted second-order polynomial regression model, which is termed a quadratic model in RSM, was used in analysing the LPBF processing parameters and the responses (as in equation 2).

$$f = a_0 + \sum_{i=1}^{n} a_i x_i + \sum_{i=1}^{n} a_{ii} x^2{}_i + \sum_{\boldsymbol{i<}}^{} \sum_{\boldsymbol{j=2}}^{\boldsymbol{n}} \boldsymbol{a_{ij} x_i x_j} + \varepsilon \tag{2}$$

where f is the predicted response, a_0 is the model intercept coefficient, a_i represents the linear effect of x_i, a_{ii} depict the quadratic effect of x_i and a_{ij} represents the linear-linear relationship between x_i and x_j, n is the number of factors (In this study n = 3), ε is residual error.

2.2 Artificial neural network (ANN)

The multilayer perceptron (MLP), feed-forward backpropagation neural network was used in this study. The training function Levenberg-Marquardt (Trainlm) and TanSigmoid transfer function (equation 3) were selected. Trainlm is an advanced nonlinear optimization algorithm. The Trainlm algorithm typically requires more memory but less time [25]. Training automatically halt when generalization cease to progress, as indicated by an increase in the mean square error of the validation sample. The sigmoid activation function is suitable for many training algorithms because it is continuous and differentiable. It varies monotonically from 0 to 1 as x varies from -∞ *to* ∞ [26].

$$f(x) = \frac{1}{1 + exp^{(-x)}} \tag{3}$$

The architecture of the network has 3 input neurons (process parameters laser power, scan speed and hatch spacing), 10 hidden layers, 4 output neurons (outputs: porosity, microhardness, amount of martensite phase composition, and wear volume) as highlighted in Figure 2.

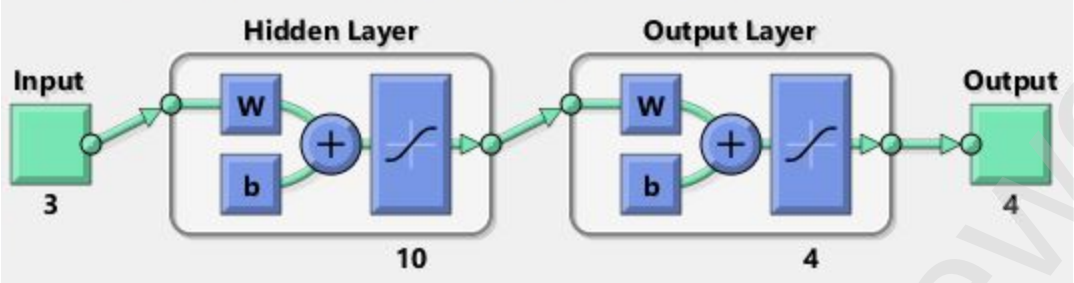

Figure 2 ANN architecture (Matlab 2019)

The training data obtained from a database of 140 data points from the 20 experiment runs (Table 5) was normalized between 0 and 1 for homogeneous attention on training (equation 4).

$$X_{norm} = \frac{X - X_{min}}{X_{max} - X_{min}} \tag{4}$$

Where X_{norm} is the normalized data, X is the observed experimental data, X_{max} is the maximum data point and X_{min} is the minimum data point. The data were categorized into the training data set 70%, validation data set 15% and testing data set 15% by dividerand data division function.

Performance of the ANN model was measured by assessing its mean squared error (MSE) and correlation coefficient (R^2). The R^2 value measures the network's accuracy to predict responses that are close to the target (experiment) values. The ANN model was trained and tested with the Neural Network Toolbox in MATLAB R2019b (9.7.0) software. The network was re-trained until accurate prediction was obtained.

3.0 Materials and Methods

3.1 Materials

The material used for LPBF process was maraging steel powder (FE 339 or DIN 1.2709) and was supplied by Praxair Surface Technologies (Connecticut, USA). The typical chemical composition of the maraging steel powder is as shown in Table 2.

(a) (b)

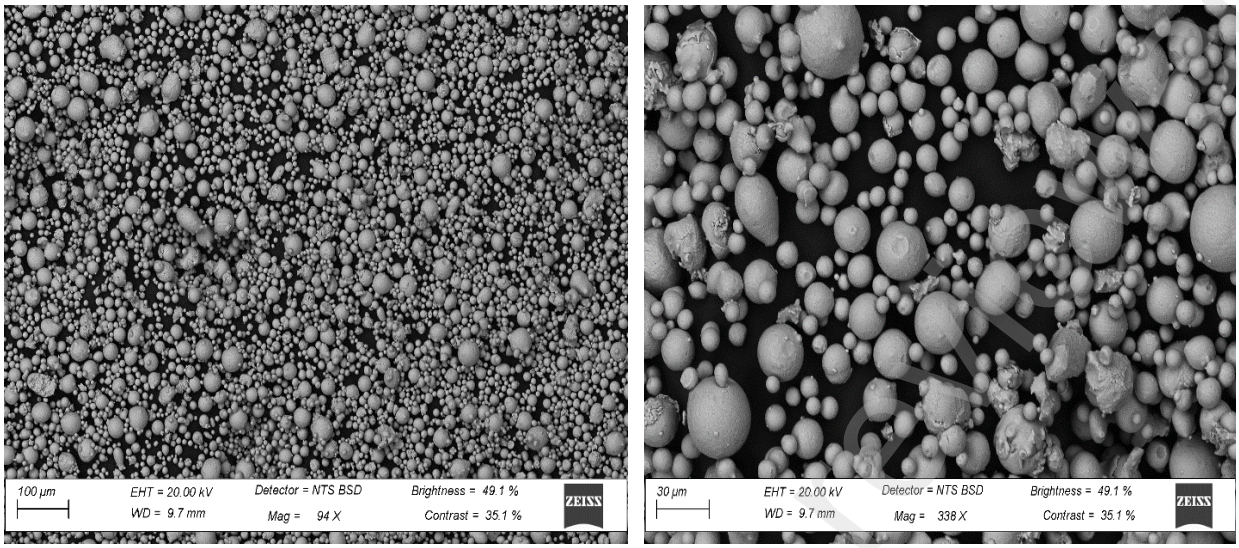

Figure 3 shows the microscopic images of the powder morphology taken with a Zeiss Merlin field emission scanning electron microscope (FE-SEM). The theoretical mechanical properties of the maraging steel parts before heat treatment are presented in Table 3.

Table 2

Chemical composition of the maraging steel powder (1.2709)

Ni	Co	Mo	Ti	Al	Cr	C	Mn, Si	P, S	Fe
17 - 19 wt%	8.5 - 9.5 wt%	4.5 - 5.2 wt%	0.6 - 0.8 wt%	0.05 - 0.15 wt%	≤ 0.5 wt%	≤ 0.03 wt%	≤ 0.1 wt% (each)	≤ 0.01 wt% (each)	balance

Table 3

Theoretical mechanical properties of maraging steel parts produced with LPBF

Properties	DIN 1.2709
Tensile strength (MPa)	1100 MPa ± 100MPa
Yield strength (0.2% MPa)	1000 MPa ± 100MPa
Elongation %	8% ± 3%
Rockwell Hardness (C-Scale)	33 – 37 HRC
Density	>99.95%

(a) (b)

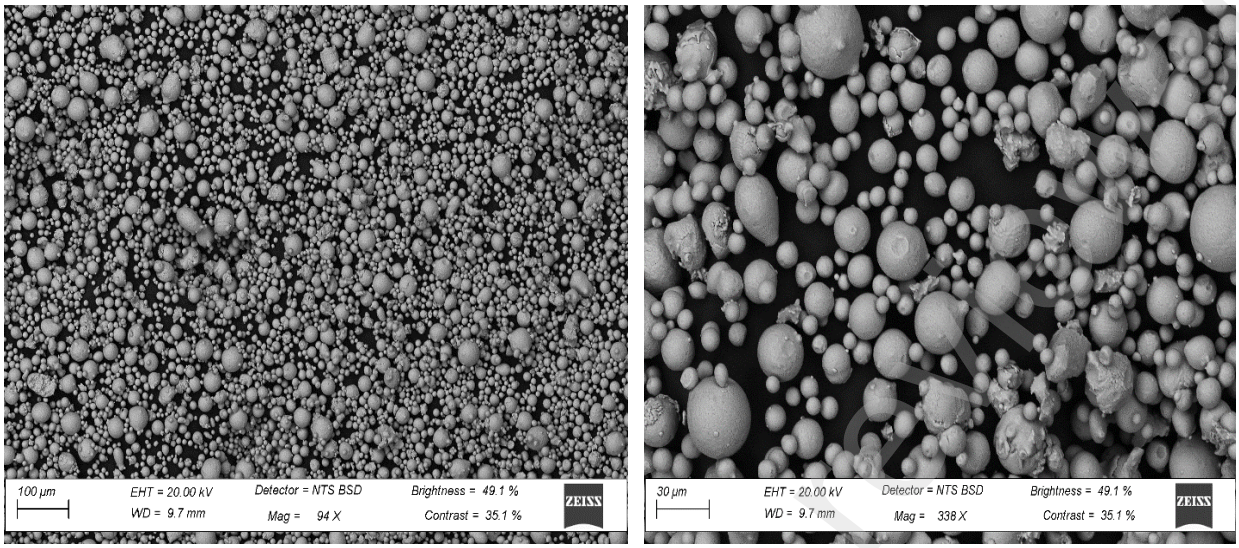

Figure 3: SEM images showing the morphology of the Praxair maraging steel (FE 339) powder at (a) 94X magnification and (b) 338X magnification

The morphology of the particles is mostly spherical with small satellite particles attached to the larger particles.

3.2 Experimental procedure

The samples were built on a Concept Laser M2 LaserCUSING machine at the Department of Industrial Engineering at Stellenbosch University. The machine specifications are presented in Table 4.

Table 4

Concept Laser M2 LaserCUSING machine specifications

Parameter	Machine specifications
Laser power	Up to 200 W
Scanning speed	Up to 5000 mm/s
Layer thickness	20-50 µm
Focus diameter	50 µm
Coater blade	Rubber
Laser system	IPG Fiber laser 200 W (cw)
Build envelope	250×250×280 mm (x,y,z)

The range of process parameters used in this work was determined upon consultation with relevant literature [27] and consultation with industrial experts at the Stellenbosch Technology Centre - Laboratory for Advanced Manufacturing (STC-LAM). Parameters that were varied included laser

power (A: 80 to 200 W), scan speed (B: 300 to 1500 mm/s) and hatch spacing (C: 60 to 120 μm). An alternating raster scan with a rotation of 90 degrees per layer and a x, y shift of 0.12 mm per layer was used. The machines build chamber was filled with nitrogen gas such that oxygen concentration was maintained below 0.2 % (2000 PPM). The samples were directly built from the baseplate without supporting structure.

The parameters were altered to investigate their influence on the microstructural properties (amount of porosity (P), microhardness (MH) and amount of martensite phase (MP)) and wear volume (WV) of LPBF fabricated maraging steel samples. Cuboid samples (with size 10 x 10 x 10 mm) were manufactured according to the experimental matrix shown in Table 5. The experimental matrix was carried out once. It is usual that such matrix optimization design is only carried out once (as in one sample per condition), particularly considering the relatively large range of parameter values and 6 parameters replicated at the central point. A similar approach was applied by [28] in optimizing the process parameters of laser powder bed fusion.

Table 5

Comparison of observed results with ANN and RSM predicted responses

Run	Power (W)	Speed (mm/s)	Hatch (μm)	Porosity (Percentage)			Microhardness (HV)			Martensite (Percentage)			Wear Volume (mm^3)		
				Expt	ANN	RSM	Expt	ANN	RSM	Expt	ANN	RSM	Expt	ANN	RSM
1	160	650	100	0.527	0.522	0.417	414.000	413.997	415.479	73.630	73.624	74.224	0.0960	0.0959	0.0989
2	170	784	95	0.858	0.820	0.791	415.600	415.583	417.996	75.168	75.074	76.258	0.0510	0.0510	0.0518
3	170	700	95	0.921	0.752	0.754	422.000	420.663	421.063	82.080	81.581	81.659	0.0826	0.0809	0.0798
4	170	700	95	0.540	0.752	0.754	424.375	420.663	421.063	83.510	81.581	81.659	0.0776	0.0809	0.0798
5	170	700	95	0.920	0.752	0.754	420.571	420.663	421.063	80.860	81.581	81.659	0.0821	0.0809	0.0798
6	170	700	95	0.450	0.752	0.754	419.250	420.663	421.063	81.960	81.581	81.659	0.0772	0.0809	0.0798
7	160	750	90	0.020	0.032	0.021	412.000	412.026	411.173	82.680	82.721	82.127	0.0649	0.0649	0.0684
8	180	750	90	0.010	0.011	-0.025	424.580	424.510	422.489	72.429	72.768	71.383	0.0717	0.0715	0.0692
9	180	650	100	1.441	1.441	1.295	410.700	410.754	410.916	80.440	80.407	80.541	0.0869	0.0869	0.0839
10	186.82	700	95	0.519	0.559	0.717	415.750	417.030	415.313	76.230	75.425	76.616	0.0787	0.0818	0.0807
11	170	700	86.60	0.36	0.38	0.499	429.91	430.00	431.13	79.15	78.82	80.07	0.077	0.077	0.075

3.3 Characterisation of LPBF fabricated samples

Experimental tests were carried out in order to investigate the effect of laser power, scan speed and hatch spacing on the porosity, microhardness, amount of martensite phase composition and wear volume of maraging steel (1.2709) parts. The samples were detached from the base plate with an AgieCharmilles CA20, wire-electrical discharge machine (W-EDM) and the cross-sections were hot mounted with PolyFast, a Phenolic hot mounting resin with carbon filler for edge retention. The mounting was done on a Struers CitoPress-5. The resin was heated to 180 °C for 3.5 minutes, at pressure of 250 bar and high cooling for 1.5 minutes. The samples were ground using a mrc MP-1B grinding and polishing machine with P1200 grit paper for the wear test and polished to 1 micron for the porosity and microhardness test.

Images of the whole cross-sectional surface were captured on an Olympus BX51M optical microscope for surface porosity analysis. The porosity analysis of the images was carried out using Stream Essentials software. The whole surface was divided into 16 portions, the Stream Essentials software analysed the 16 images for porosity and computed an average percentage porosity of the surface.

The microhardness values of cross-section surface of the parts were tested using a Zwick Roell ZHVμ Vickers hardness tester under the load of 1000 gf with the load-dwell time of 10 seconds. The microhardness was measured manually by changing the camera magnification from 10x to 40x. The average values were obtained at 12 different locations uniformly distributed on the cross-sectional surface of each sample.

Wear tests were performed with a Rtec Universal tribometer using Silicon Nitride wear balls. The ball size was ∅6.35mm, with a 150N load, a velocity of 1 mm/s, an acceleration of 0.1 mm/s², a time of 10 minutes, and a sliding distance of 2 mm. The wear tracks were observed and the wear scar length (Y) and width (X) were measured with a Nikon ECLIPSE 50i POL optical microscope fitted with a digital camera. The width (X) was also measured with the Rtec Universal tribometer analysis application suite. The wear volume of the wear scar was calculated by using Equations 5, 6 and 7 [29].

$$V_f = L_s\left[{R_f}^2 \sin^{-1}\left(\frac{W}{2R_f}\right) - \frac{W}{2}(R_f - h_f)\right] + \pi\frac{(L - L_s)}{3W}\left[{h_f}^2(3R_f - h_f)\right] \quad (5)$$

$$h_f = R_f - \sqrt{{R_f}^2 - \frac{W^2}{4}} \quad (6)$$

$$R_f = \left(\frac{L - L_s}{2}\right) \quad (7)$$

where V_f is the wear volume, L_s is the stroke length of the sliding wear ball, L is the length of the wear scar, W is the width of the wear scar, h_f is the wear depth and R_f is the radius of the spherical surface at both ends of the wear scar.

X-ray diffraction (XRD) patterns were measured with a Bruker D8 Advance. The machine was set at the following parameters; Voltage: 40KV, Current: 40mA, Power: 16000W, X-ray source: Cu tube, Detector: LYNXEYE, Scan type: Coupled 2 theta/theta from 20° to 90°, Scan mode: Continuous PSD fast. Phase quantification was carried with Diffrac.EVA V3.1 software.

4.0 Results and discussion

The developed RSM and ANN models can correlate the LPBF process parameters to the microstructural characteristics and wear resistance of maraging steel (1.2709) parts.

4.1 Response surface modelling (RSM) analysis and validation

Table 5 shows the outcome of the RSM analysis of the experimental data. Analysis of variance (ANOVA) and regression analysis were performed in this section to evaluate the significance of the model.

4.1.1 Analysis of variance (ANOVA)

4.1.1.1 Percent porosity (P) of the LPBF fabricated maraging steel samples

Analysis of variance (ANOVA) was performed using Minitab 17 software to evaluate the significance of the model, the crucial effect of the individual variables and combined variables. The significant model terms were determined via a stepwise regression procedure which automatically removes the insignificant terms. Based on the ANOVA analysis for porosity responses (Table 6), it is notable that the model was statistically significant with a large F-value of 16.45 and p-value < 0.05. Factors with a large F-value and p-value < 0.05 are considered significant. The most significant model factors for porosity were all three parameters (laser power (A), scan speed (B) and hatch spacing (C)). The combined parameters laser power * laser power (A^2), scan speed * scan speed (B^2), laser power * scan speed, (AB) laser power * hatch spacing (AC) and scan speed * hatch spacing (BC) were also statistically significant. A coefficient of determination R^2 value of 0.9229, adjusted R^2 value of 0.8668 and predicted R^2 value of 0.6792 were obtained.

Table 6

ANOVA and Response Surface Regression for % Porosity

Source	Sum of squares	df	Mean squares	F-value	P-value prob>F
Model	5.9506	8	0.74383	16.45	< 0.000 significant
Linear	1.8560	3	0.61865	13.68	0.000
A	0.5910	1	0.59103	13.07	0.004
B	0.7450	1	0.74503	16.48	0.002
C	0.5199	1	0.51989	11.50	0.06
Square	0.6674	2	0.33371	7.38	0.009
A^2	0.2833	1	0.28331	6.27	0.029
B^2	0.3242	1	0.32421	7.17	0.021
2-way interaction	3.4273	3	1.14242	25.27	0.000
AB	0.4979	1	0.49785	11.01	0.007
AC	1.8467	1	1.84675	40.85	0.000
BC	1.0826	1	1.08265	23.95	0.000
Residual error	0.4973	11	0.04521		
Lack of Fit	0.2511	6	0.04185	0.85	0.583 not significant
Pure Error	0.2462	5	0.04924		
Cor Total	6.4479	19			
Std. Dev.	0.212621				
R^2		0.9229			
Adjusted R^2		0.8668			
Predicted R^2		0.6792			

The R^2 value indicates good correlation between the experimental and predicted data obtained for porosity as indicated in Figure 4. The difference between the adjusted R^2 and the predicted R^2 is < 0.2 indicating that they are in reasonable agreement. The regression (equation 8) describes the empirical relationship between the porosity and the LPBF processing parameters after eliminating non-significant factors with the standard deviation of ± 0.21 of the mean value of porosity.

$$\% \text{ Porosity} = 298.2 - 0.767\ A - 0.3130\ B - 2.625\ C - 0.001395\ A^2 + 0.000060\ B^2 + 0.000499\ BC + 0.00961\ AC + 0.001471\ BC \quad (8)$$

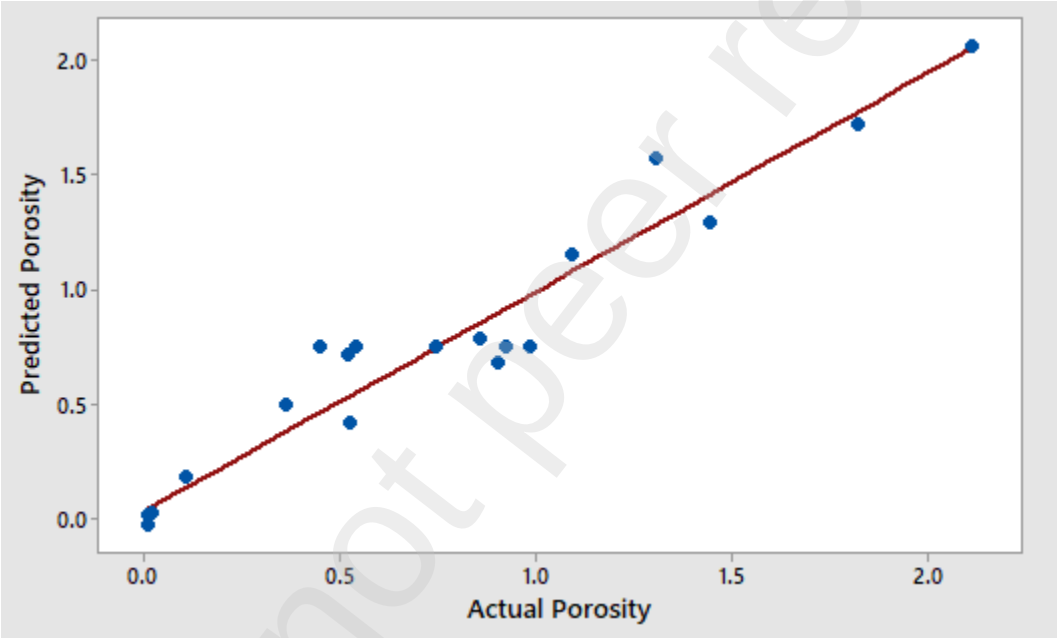

Figure 4. Predicted vs measured values of % porosity

4.1.1.2 Microhardness (MH) of the LPBF fabricated maraging steel samples

The results from the ANOVA for microhardness responses can be observed in Table 7, which suggests that the model was statistically significant with a large F-value of 27.99 and p-value < 0.05. Factors with a large F-value and p-value < 0.05 are considered significant. All the three parameters were found to be significant model factors that influence microhardness. The combined parameters laser power * laser power (A^2), hatch spacing * hatch spacing (C^2), Power*Speed (AB), and Speed*Hatch (BC) were also statistically significant. A coefficient of determination R^2 value of 0.9423, adjusted R^2 value of 0.9086 and predicted R^2 value of 0.8205 were obtained.

Table 7

ANOVA and Response Surface Regression for Microhardness

Source	Sum of squares	df	Mean squares	F-value	P-value prob>F
Model	889.48	7	127.069	27.99	< 0.000 significant
Linear	401.41	3	133.804	29.47	0.000
A	38.92	1	38.917	8.57	0.013
B	93.76	1	93.756	20.65	0.001
C	268.74	1	268.741	59.19	0.000
Square	157.97	2	78.985	17.40	0.000
A^2	138.38	1	138.379	30.48	0.000
C^2	11.23	1	11.225	2.47	0.142
2-way interaction	330.10	2	165.049	36.35	0.000
AB	174.35	1	174.351	38.40	0.000
BC	155.75	1	155.746	34.31	0.000
Residual error	54.48	12	4.540		
Lack of Fit	34.78	7	4.968	1.26	0.413 not significant
Pure Error	19.70	5	3.940		
Cor Total	943.96	19			
Std. Dev.	2.13072				
R^2		0.9423			
Adjusted R^2		0.9086			
Predicted R^2		0.8205			

The R^2 value of 0.9423 is very close to 1, which indicates good correlation between the experimental and predicted data obtained for microhardness as indicated in Figure 5. The difference between the adjusted R^2 and the predicted R^2 is < 0.2 indicating that they are in reasonable agreement. The regression equation (9) describes the empirical relationship between the microhardness and the LPBF processing parameters after eliminating non-significant factors with the standard deviation of ± 2.13 of the mean value of microhardness.

$$\text{Microhardness} = 2225 + 4.12\,A - 3.316\,B - 19.93\,C - 0.03083\,A^2 + 0.0352\,C^2 + 0.00934\,AB + 0.01765\,BC \quad (9)$$

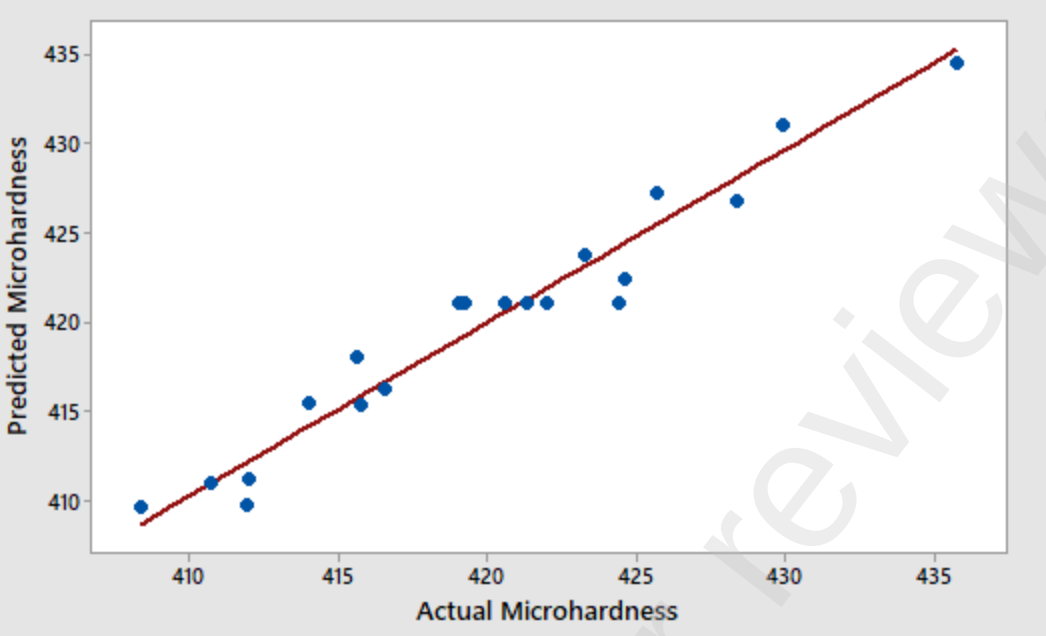

Figure 5 Predicted vs measured values of microhardness

4.1.1.3 Amount of martensite phase (MP) of the LPBF fabricated maraging steel samples

The model large F-value of 16.12 and p-value < 0.05 as shown in ANOVA Table 8, shows that the model is significant. Processing parameters with a large F-value and p-value < 0.05 are considered significant. Laser power was found to have the most significant effect on the martensite phase composition considering its F-value of 15.10 and p-value of 0.003. The combined parameters Power*Power (A^2), Speed*Speed (B^2), Hatch*Hatch (C^2), Power*Speed (AB), Power*Hatch (AC) and Speed*Hatch (BC) were also statistically significant. A coefficient of determination R^2 value of 0.9355, adjusted R^2 value of 0.8775 and predicted R^2 value of 0.7374 were obtained.

Table 8

ANOVA and Response Surface Regression for % Martensite

Source	Sum of squares	df	Mean squares	F-value	P-value prob>F
Model	160.765	9	17.8628	16.12	< 0.000 significant
Linear	17.557	3	5.8523	5.28	0.019
A	16.729	1	16.7293	15.10	0.003
B	0.738	1	0.7377	0.67	0.434
C	0.090	1	0.0897	0.08	0.782
Square	59.335	3	19.7783	17.85	0.000
A^2	18.240	1	18.2398	16.46	0.002
B^2	45.262	1	45.2624	40.85	0.000
C^2	3.789	1	3.7894	3.42	0.094
2-way interaction	83.873	3	27.9578	25.23	0.000
AB	37.980	1	37.9795	34.28	0.000
AC	34.823	1	34.8233	31.43	0.000
BC	11.071	1	11.0706	9.99	0.010
Residual error	11.080	10	1.1080		
Lack of Fit	4.653	5	0.9306	0.72	0.634 not significant
Pure Error	6.427	5	1.2853		
Cor Total	171.845	19			
Std. Dev.	1.05261				
R^2		0.9355			
Adjusted R^2		0.8775			
Predicted R^2		0.7374			

The good correlation between the experimental and predicted data obtained for percentage martensite phase composition was observed based on the R^2 value, this was further indicated by plot diagram in Figure 6. The difference between the adjusted R^2 and the predicted R^2 is < 0.2 indicating that they are in reasonable agreement. The regression equation (10) describes the empirical relationship between the amount of martensite phase composition and the LPBF processing parameters after eliminating non-significant factors with the standard deviation of ± 1.05 of the mean value of martensite phase composition.

$$\%\text{Martensite} = -288 + 2.80\,A + 1.283\,B - 6.47\,C - 0.01125\,A^2 - 0.000710\,B^2 - 0.0205\,C^2 - 0.004358\,AB + 0.04173\,AC + 0.00471\,BC \quad (10)$$

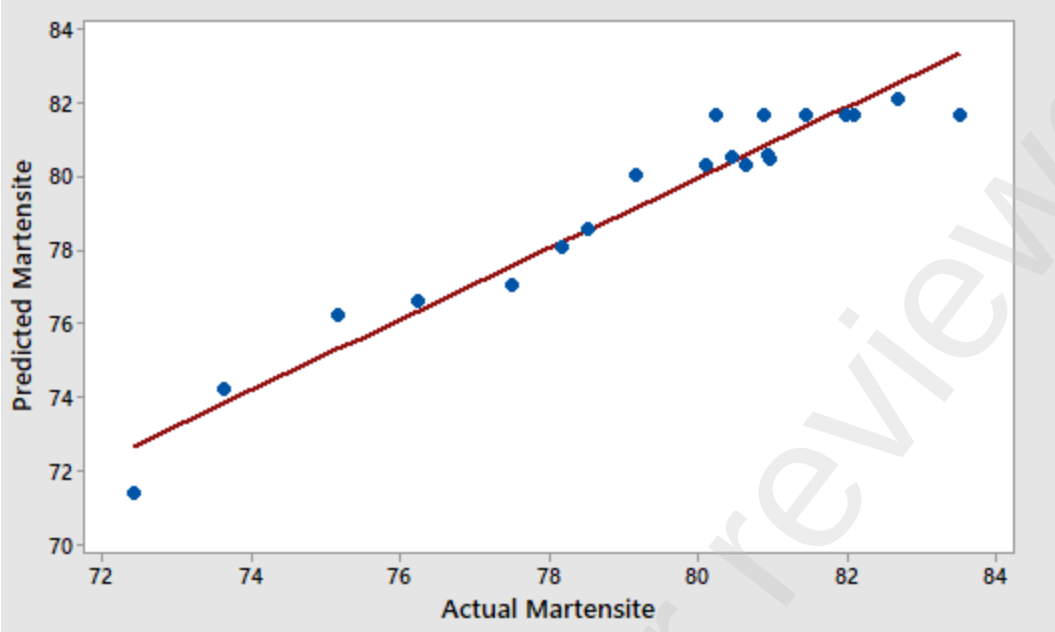

Figure 6 Predicted vs measured values of % martensite

4.1.1.4 Wear volume (WV) of the LPBF fabricated maraging steel samples

An ANOVA was performed to evaluate the significance of the model for wear volume responses (Table 9), high F-value of 25.88 and p-value < 0.05 of the model indicates that it is significant. All the three parameters were significant in the model for wear volume since their F-value is large and p-value < 0.05. The combined parameters Power*Power (A^2), Speed*Speed (B^2), Power*Speed (AB) and Speed*Hatch (BC) were also statistically significant. Further discussion on the influence of the single and combined factors was highlighted with the main effects and contour plots in the following sections.

Table 9

ANOVA and Response Surface Regression for Wear volume

Source	Sum of squares	df	Mean squares	F-value	P-value prob>F
Model	0.002000	7	0.000286	25.88	< 0.000 significant
Linear	0.001138	3	0.000379	34.38	0.000
A	0.000172	1	0.000172	15.57	0.002
B	0.000774	1	0.000774	70.09	0.000
C	0.000193	1	0.000193	17.48	0.001
Square	0.000560	2	0.000280	25.37	0.000
A^2	0.000080	1	0.000080	7.22	0.020
B^2	0.000442	1	0.000442	40.04	0.000
2-way interaction	0.000301	2	0.000151	13.64	0.001
AB	0.000252	1	0.000252	22.82	0.000
BC	0.000049	1	0.000049	4.46	0.056
Residual error	0.000132	12	0.000011		
Lack of Fit	0.000098	7	0.000014	2.01	0.231 not significant
Pure Error	0.000035	5	0.000007		
Cor Total	0.002132	19			
Std. Dev.	0.0033223				
R^2		0.9379			
Adjusted R^2		0.9016			
Predicted R^2		0.7798			

A coefficient of determination R^2 value of 0.9379, which is closer to 1, indicates good correlation between the experimental and predicted data obtained for porosity as indicated in Figure 7. The difference between the adjusted R^2 value of 0.9016 and predicted R^2 value of 0.7798 is < 0.2 indicating that they are in reasonable agreement. The empirical relationship between the wear volume and the LPBF processing parameters after eliminating non-significant factors with the standard deviation of ± 0.0033 of the mean value of wear volume is described by the regression equation (12).

$$\text{Wear Volume} = 0.445 - 0.01617\,A + 0.001976\,A + 0.00770\,C + 0.000023\,A^2 - 0.000002\,B^2 + 0.000011\,AB - 0.000010\,BC \quad (11)$$

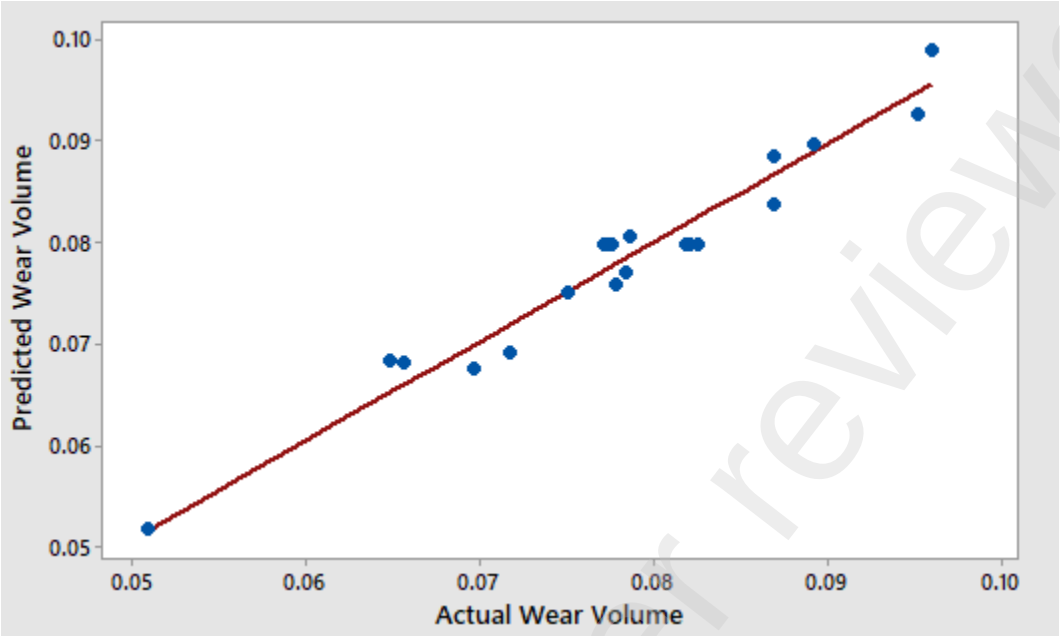

Figure 7 Predicted vs measured values of wear volume

4.2 Influence of LPBF process parameters on the sample properties

Main effects and contour plots are presented in the following sections. They describe how laser power, scan speed and hatch spacing affect the porosity, microhardness, amount of martensite phase and wear volume of maraging steel (1.2709) parts.

4.2.1 Influence of LPBF process parameters on porosity

The main effects plot presented in Figure 8 describes how laser power (A), scan speed (B) and hatch spacing (C) affect porosity of the samples. The main effects plot indicates that micro-porosity in the samples increases as laser power increases from 160 W to 177.5 W (Figure 8a). This is contrary to expectation that porosity is reduced as laser power increases [8], According to Mugwagwa *et al.,* [27], this could be attributed to the mismatch between the process parameters. By increasing the laser power above 177.5 W (Figure 8a), the porosity is seen to decrease. This could be attributed to the energy dissipated to the melt pool, the energy would be sufficient to completely melt the powders [7] but not too much to cause over melting and balling of the melt pool [27]. Figure 9 (a to c) support the outcome reported in Figure 8a. Meanwhile, it is also evident from Figure 9 (a to b) that laser power, besides influencing the amount of porosity imparted in the

LPBF fabricated sample, also determines the pore morphology, the pore size and the inter-pore spacing. According to Figure 9 (a and b), it is evident that pore sizes increase (0 to 50 μm) , the inter-pore spacing (250 μm) decreases while the pores are non-uniformly distributed within the microstructure when laser power less than 177.5 W is selected to dissipate heat into the melt pool. However, by dissipating heat into the melt pool with a laser power set above 177.5 W, the pore size reduces (10 μm), the inter-pore spacing (400 μm) increases while the pores are more uniformly distributed (Figure 9c).

A study of Figure 8b indicates that as scanning speed (B) is increased from 650 mm/s to 738 mm/s, the porosity is seen to decrease to the minimum value. This could be attributed to over melting and balling at speeds lower than 738 mm/s [27]. By increasing the scanning speed above the threshold value of 738 mm/s, the porosity increases due to a decrease in the width of the melt pool at higher scanning speed [27]. The energy density delivered to the melt pool would be insufficient for complete melting of the powders [7] hence the increase in porosity. It is clear from Figure 9 (d and e) that pore sizes reduce (0 to 50 μm), the inter-pore spacing (250 μm) increases while the pores appear to be uniformly distributed within the microstructure when the value of scanning speed tends towards 738 mm/s. By scanning laser beam at a speed greater than 738 mm/s, the pore size increases (10 μm), the inter-pore spacing (400 μm) reduces while the pores appear non- uniformly distributed (Figure 9f).

The main effect plot Figure 8c indicates that as hatch spacing is increased from 87 μm to 103 μm, the porosity is seen to increase to the maximum value. This could be due to decreased energy density dissipated to the melt pool as the hatch spacing is increased. The energy density would be insufficient for complete melting of the powders [7] hence the increase in porosity. The optical microscope images (Figure 9 g to h) support the outcome reported in Figure 8c.

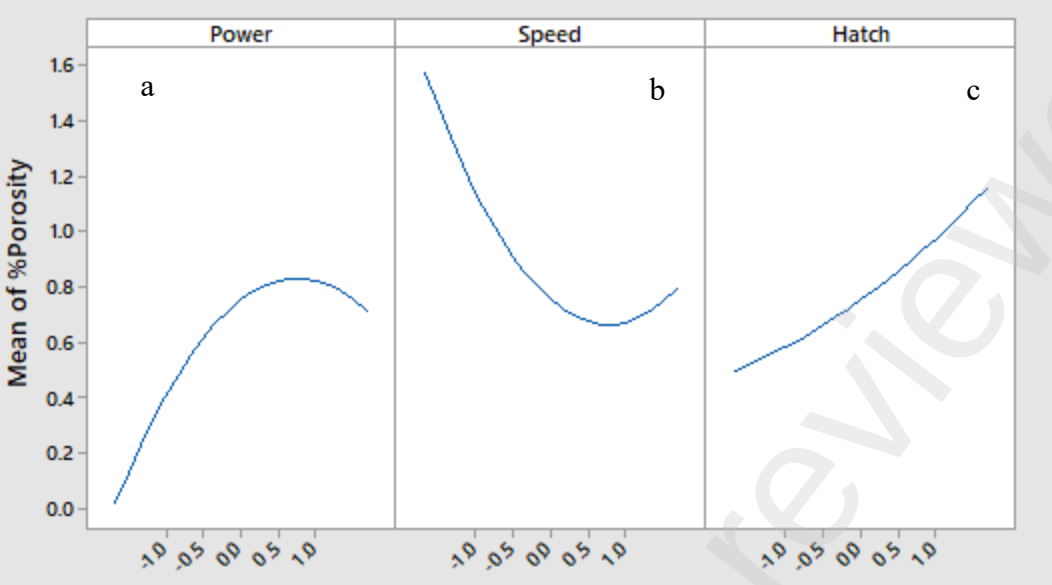

Figure 8 Main effects plot for the influence of all parameters on porosity

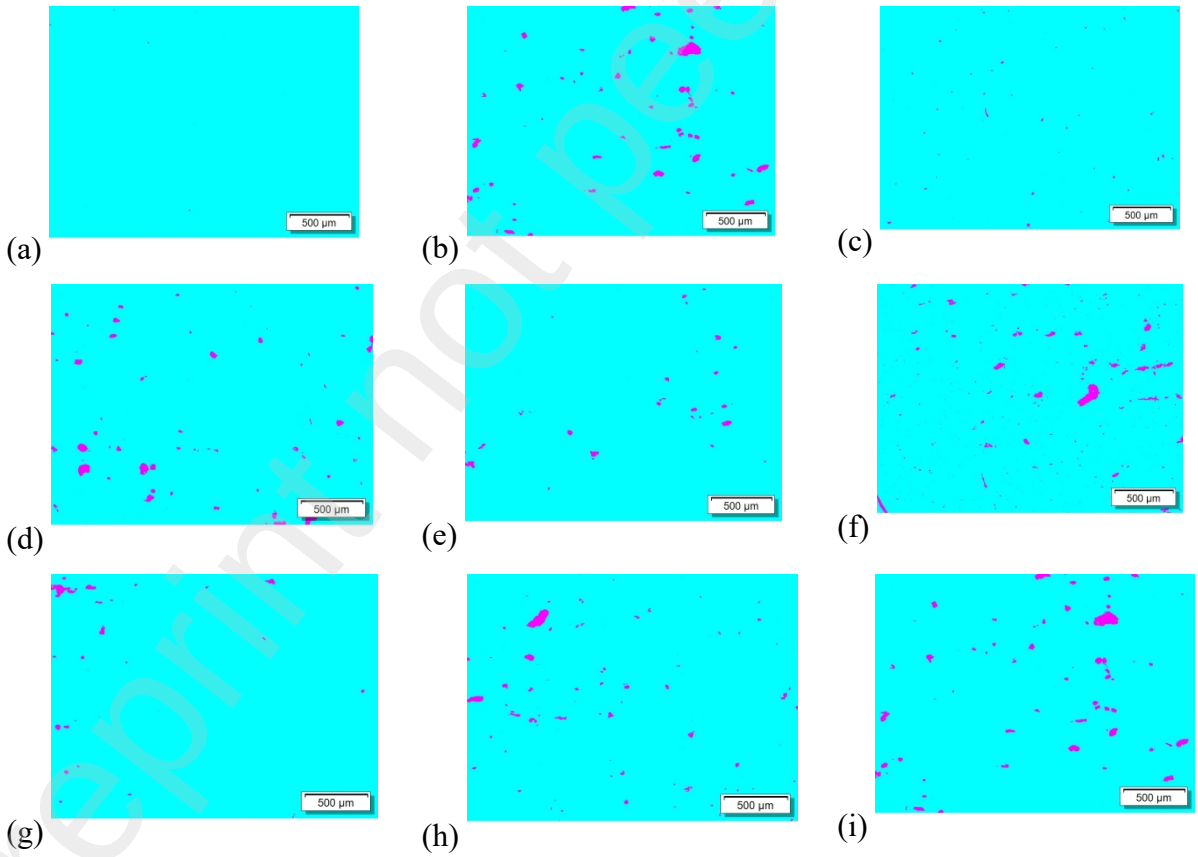

Figure 9: Porosity analysis of LPBF fabricated samples as a function of laser power (a) 153 W, (b) 170 W, (c) 187 W; scanning speed (d) 616 mm/s, (e) 700 mm/s, (f) 784 mm/s; hatch spacing (g) 87 µm, (h) 95 µm and (i) 103 µm

The effects of the interaction between laser power and scan speed, scan speed and hatch spacing, as well as laser power and hatch spacing on porosity were presented in contour plots Figure 10a, Figure 10b and Figure 10c respectively. The contour plot describes the interaction between two parameters holding the third parameter at zero level. A porosity < 0.4 % is obtained when the scan speed is set above 725 mm/s whilst setting power <163 W, as presented in Figure 10a. Less porosity (<0.5%) is also observed when speed is set above 725 mm/s and hatch spacing <91.25 μm as shown in Figure 10b. Less porosity (<0.2) is observed when power is >180 W and hatch spacing <90 μm Figure 10c.

(a)

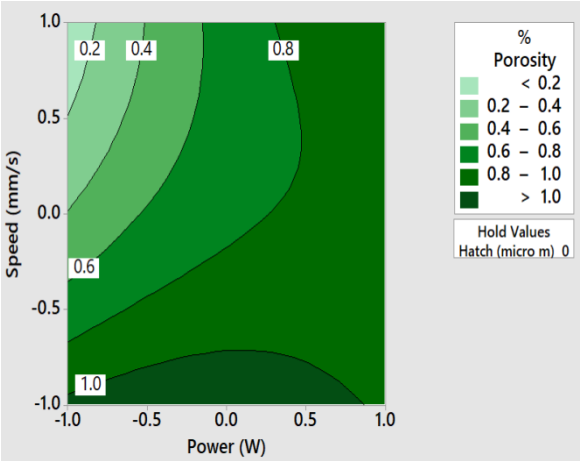

(b)

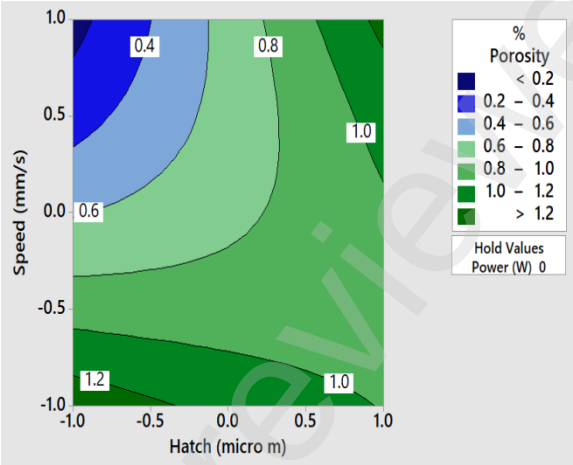

(c)

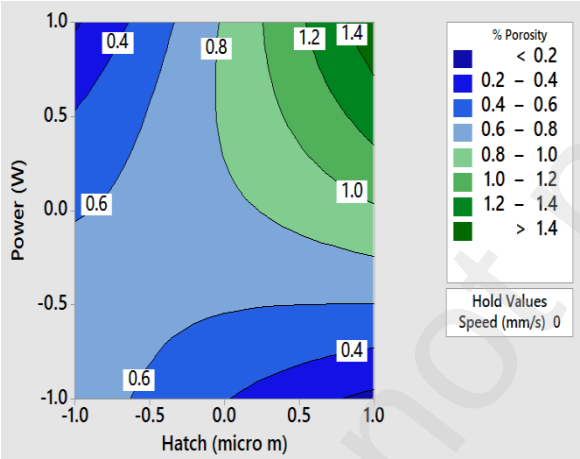

Figure 10 (a) Contour plot of the influence of laser power and scan speed on porosity (b) Contour plot of the influence of hatch spacing and scan speed on porosity (c) Contour plot of the influence of hatch spacing and laser power on porosity

4.2.2 Influence of LPBF process parameters on microhardness

Figure 11 shows the influence of laser power (A), scan speed (B) and hatch spacing (C) on microhardness of the LPBF manufactured samples. The results obtained for microhardness Figure 11 a and b are contrary to the porosity results Figure 8 a and b because, whenever possible, the microhardness was measured at pore free locations [1]. The main effects plot Figure 11a shows

that with increasing the laser power from 153.2 W to 170 W the microhardness increases to the maximum. This could be attributed to increase in energy density, the energy dissipated to the melt pool would completely melt the powders [7], hence the increase in microhardness. By increasing the laser power above 170W (Figure 11a), the microhardness is seen to decrease. This could be attributed to over melting and balling at power inputs higher than 170 W [27]. The microhardness distribution graphs Figure 12 a to c support the findings on Figure 11 a. It is evident from Figure 12 a to c that laser power influenced microhardness distribution, the distribution changed from heterogeneous at 153 W (Figure 12a) to homogeneous at 170 W (Figure 12b) and heterogeneous again at 187 W (Figure 12c).

The main effect plot Figure 11b indicates that as scanning speed (B) is increased from 616 mm/s to 784 mm/s, the microhardness is seen to decrease to the minimum value. The microhardness decreases with the increase in scan speed Figure 11b. Yasa et al., [7] obtained a similar pattern on the effect of scan speed on microhardness. However, their study stated that change of scan speed does not have a significant influence on microhardness within the low speed range. This would be due to reduction in the supplied energy density as the scan speed is increased [30]. The energy density delivered to the melt pool would be insufficient for complete melting of the powders [7] hence the decrease in microhardness. Decrease in the microhardness would also be attributed to the microhardness distribution. Figure 12 d to f indicates that the microhardness distribution changed from homogeneous to heterogeneous.

The main effect plot Figure 11c indicates that as hatch spacing (C) is increased from 87 μm to 103 μm, the microhardness is seen to reduce to the minimum value. This could also be attributed to reduction in the supplied energy density as the hatch spacing is increased [30]. The hatch spacing has noticeable influence on microhardness distribution. The distribution changed from fairly homogeneous at 86.6 μm (Figure 12g) to heterogenous at 95 μm (Figure 12h) and homogenous at 103.4 μm (Figure 12i).

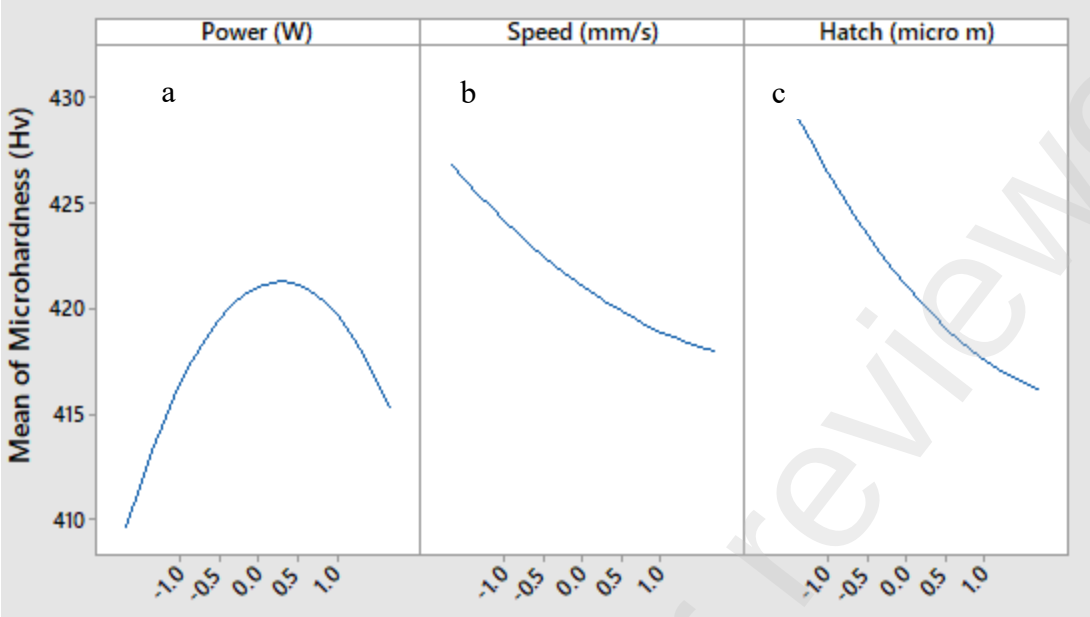

Figure 11 Main effects plot for the influence of all parameters on microhardness

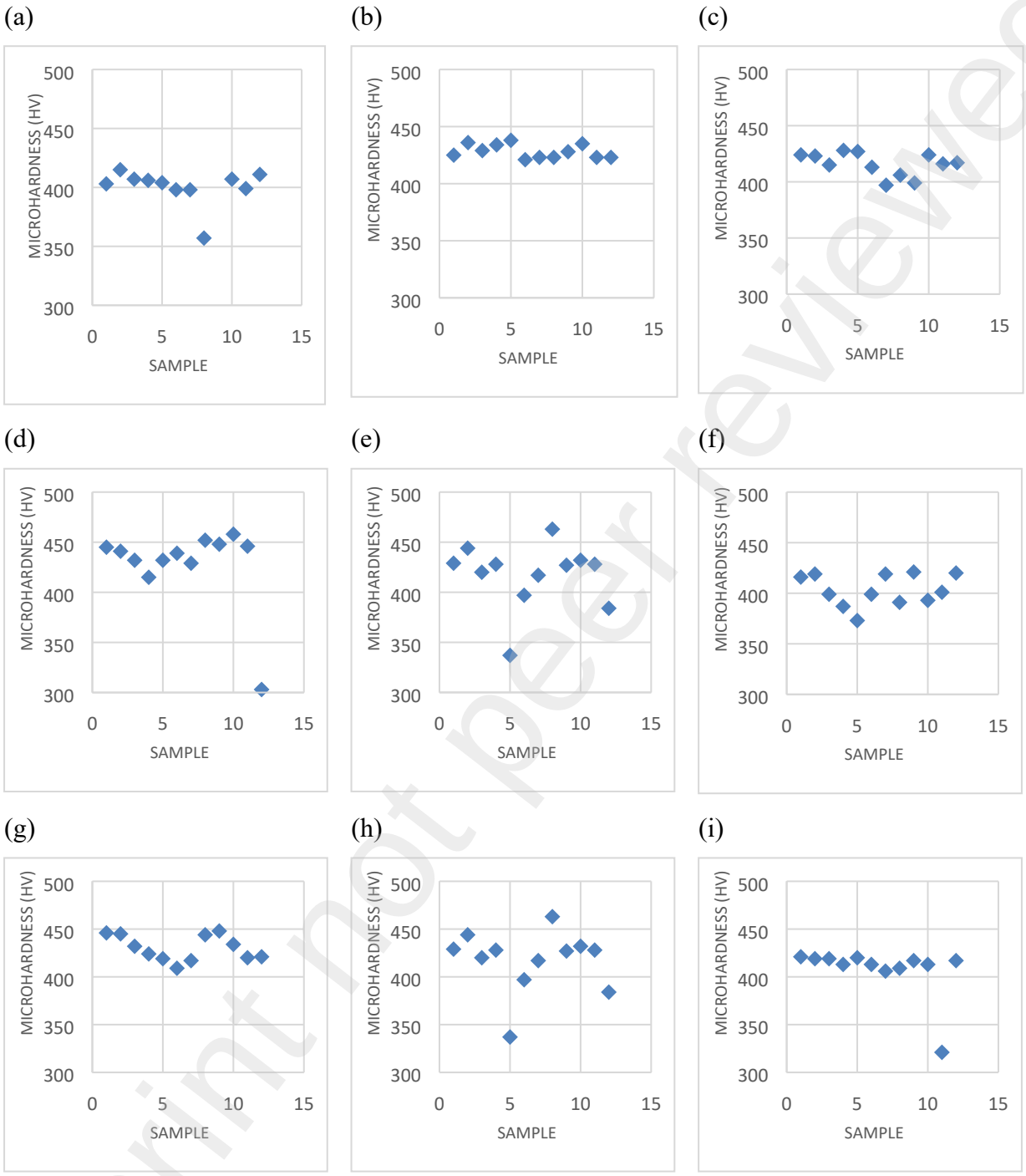

Figure 12 Microhardness distribution on LPBF fabricated samples as a function of laser power (a) 153 W, (b) 170 W, (c) 187 W; scanning speed (d) 616 mm/s, (e) 700 mm/s, (f) 784 mm/s; hatch spacing (g) 86.6 µm, (h) 95 µm and (i) 103.4 µm

Figure 13a and b show the 2D contour plots of the interactive effect of the significant parameters on microhardness: scan speed vs laser power and scan speed vs hatch spacing respectively. Figure

13a was developed with scan speed and laser power being varied whilst setting hatch spacing at centre point. At scan speed < 663 mm/s and laser power < 174 W, a high microhardness was observed (> 422.5HV). Figure 13b shows that high microhardness (> 432HV) was also observed at low speed value (663 mm/s) and low hatch spacing (91 µm).

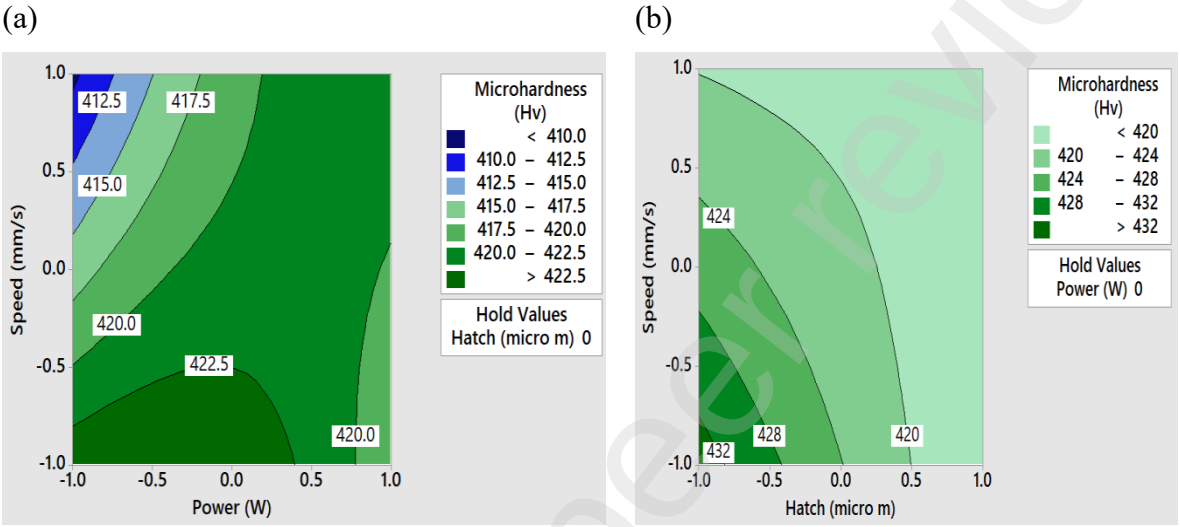

Figure 13 (a) Contour plot of the influence of scan speed and laser power on microhardness (b) Contour plot of the influence of hatch spacing and scan speed on microhardness

4.2.3 Influence of LPBF process parameters on the amount of martensite phase composition

Amount of martensite phase composition significantly influences strength and hardness of maraging steel whilst amount austenite influences ductility and toughness [31], [32], [33]. This implies that amount of martensite influences wear volume since it has significant influence on microhardness [34]. The martensitic matrix is strengthened by intermetallic nano-precipitates formed in the martensite matrix [35], [33]. The precipitated particles will hamper the movement of dislocations thereby strengthening the steel [6].

The influence of laser power (A), scan speed (B) and hatch spacing (C) on the amount of martensite phase composition of the samples is presented by main effects plot Figure 14 a to c. The XRD analysis results of manufactured samples showed that the samples consisted of a large amount of

martensite and a small amount of austenite phase composition because of the rapid cooling rates experienced during the LPBF process. The main effects plot Figure 14a shows that with increasing the laser power from 153 W, the martensite phase composition increases to the maximum amount until a laser power of 165 W is reached. Maximum amount of martensite was obtained at 165 W, as the melt pool temperature was sufficient to convert the austenite to a martensitic phase. Micro-segregation of nickel solute element at cellular boundaries during solidification stabilized the small amount of austenite phase [36]. The large amount of martensite obtained at 165 W can also be attributed to a reduced cooling rate due to increase in laser energy density [37]. By increasing the laser power above 165 W the amount of martensite phase composition is seen to decrease due to the increase in melting temperature that results in reversion of the martensite phase into the austenite phase [35].

Figure 14b shows that with increasing the scan speed, the amount of martensite phase composition increases to the maximum until scan speed of 700 mm/s. The phase composition reduces when the scan speed is increased above 700 mm/s. The temperature would be insufficient to convert austenite to martensite phase due to a decrease in the width of the melt pool at higher scanning speed. High scanning speed at constant laser power and hatch spacing reduces laser energy input, reducing cooling rate during solidification thereby reducing the martensite lath size [37].

The amount of martensite phase composition increases to maximum volume fraction as hatch spacing increases from 86 μm to 96 μm (Figure 14c). Percent volume of martensite phase composition is low at hatch spacing lower than 96 μm because the large temperature produced at the high energy density could cause the reversion of the martensite phase into the austenite phase. By increasing the hatch spacing above 96 μm, the amount of martensite phase composition is seen to decrease. This could be due to a reduction in the supplied energy density as the hatch spacing is increased hence the temperature would be insufficient for austenite to martensite phase conversion [37].

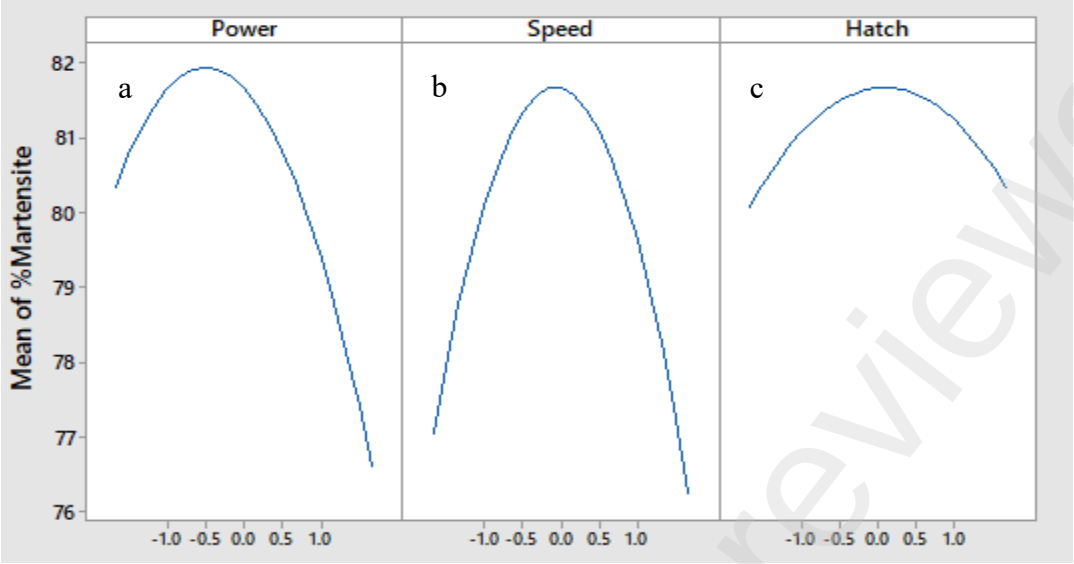

Figure 14 Main effects plot for the influence of all parameters on martensite phase composition

Figure 15a, b and c represent the interactive influence of two parameters on the martensite phase composition whilst keeping the other parameter constant. Between 713 mm/s and 738 mm/s scanning speed , the martensite phase would be >82% when laser power < 165 W (Figure 15a). When scan speed is at 700 mm/s (zero level), martensite phase would be > 81 % despite the hatch spacing (Figure 15b). Figure 15c shows that > 82% martensite phase would be obtained at laser power < 675 W and hatch spacing < 94 μm.

(a)

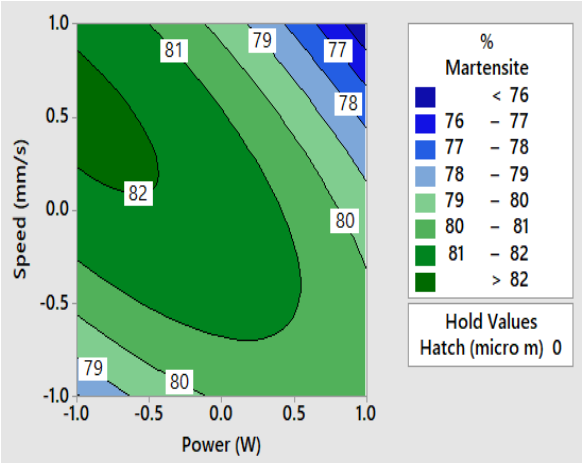

(b)

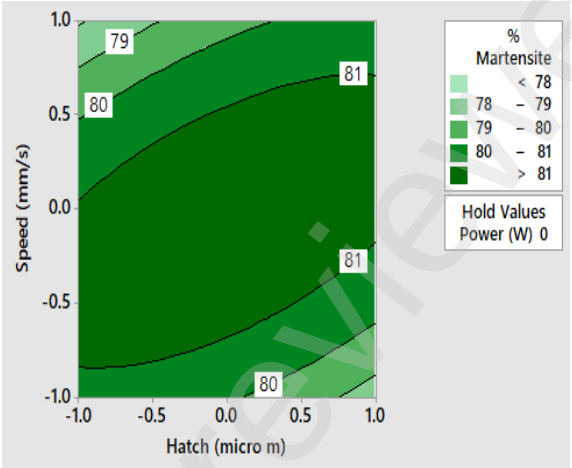

(c)

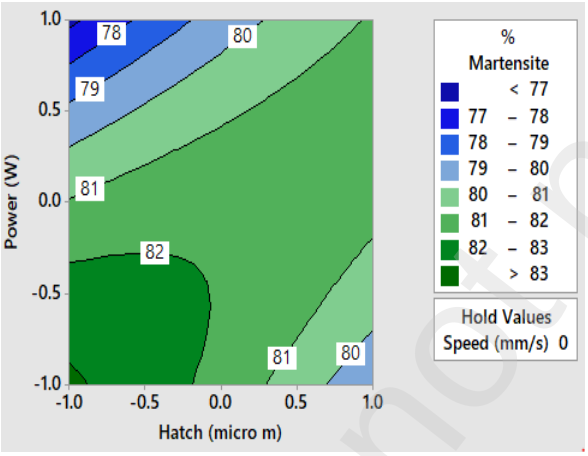

Figure 15 (a) Contour plot of the influence of scan speed and laser power on martensite phase composition (b) Contour plot of the influence of scan speed and hatch spacing on martensite phase composition (c) Contour plot of the influence of laser power and hatch spacing on martensite phase composition

4.2.4 Influence of LPBF process parameters on wear volume

Figure 16 is a main effects plot which describes how laser power (A), scan speed (B) and hatch spacing (C) affects wear volume of the samples. The main effects plot (Figure 16a) indicates that with increasing the laser power from 153 W, the wear volume decreased to the minimum until certain value of laser power (178 W) was reached. The wear volume was observed to be increasing

when the power value exceeds 178 W. This would be attributed to the microhardness of the sample (Figure 11a) and amount of martensite phase composition (Figure 14a). From section 4.2.3, amount of martensite phase composition significantly influences material hardness, strength, ductility and toughness [31], [32], [33]. The hardness significantly affects the wear resistance of a material [34]. Within the tested power range, effect of porosity (Figure 8a) was overridden by the corresponding amount of martensite and microhardness.

Figure 16b indicates that wear volume in the samples increases as the scanning speed increases from 616 mm/s to 675 mm/s. This is opposed to the expected pattern of wear volume decreasing to a minimum then increase again due to the corresponding porosity (Figure 8b) and phase composition (Figure 14b). This could be attributed to the corresponding microhardness (Figure 11b) that had resulted from the mismatch between the process parameters. By increasing the scanning speed above 675 mm/s (Figure 16b), the wear volume is seen to decrease. Meanwhile Figure 12d to f suggest that the wear pattern could be due to the microhardness distribution at the different scanning speeds. The wear volume increased to maximum as the microhardness changed from homogeneous distribution at 616 mm/s (Figure 12d) to heterogeneous distribution at 700 mm/s (Figure 12e). Beyond that point the wear volume reduced as the microhardness changed to fairly homogeneous distribution again at 784 mm/s (Figure 12f).

The main effect plot Figure 16c indicates that as hatch spacing (C) is increased from 87 μm to 103 μm, the wear volume is seen to increase to the maximum value. This could be attributed to the corresponding reduction in microhardness (Figure 11c) and an increase in porosity (Figure 8c). The increase in wear volume as the amount of martensite increase (Figure 14c) may be attributed to the brittleness of the martensite phase. A further increase in the wear volume would be attributed to the increase in volume of the soft austenite phase.

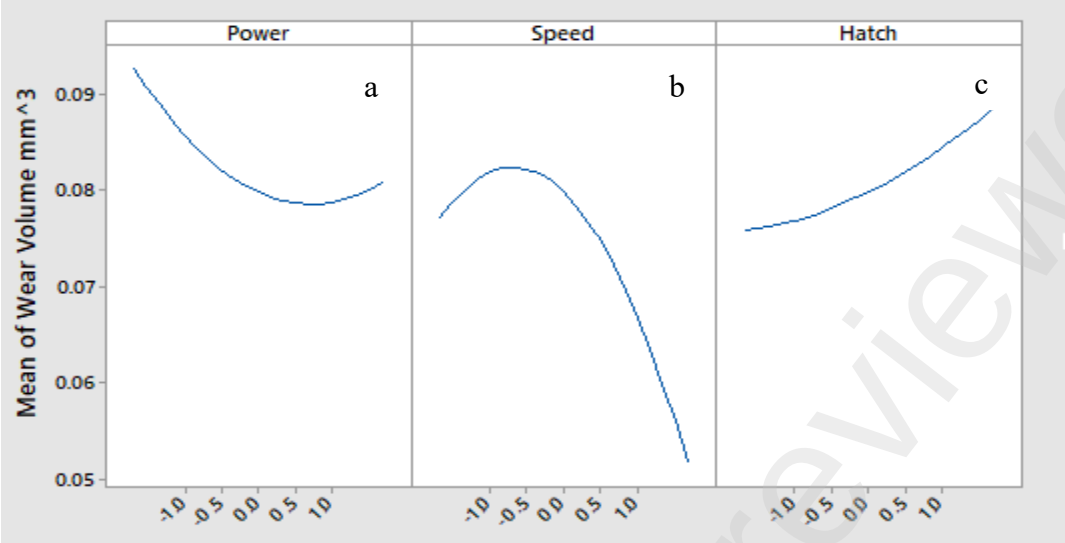

Figure 16 Main effects plot for the influence of all parameters on wear volume

The interaction between the significant factors for wear volume namely: scan speed with laser power (AB) and scan speed with hatch spacing (BC) are presented in Figure 17a and b respectively. The interaction between the two factors on wear volume was observed whilst holding the third value at a constant centre value. Minimum wear volume (< 0.07mm³) would be obtained when scan speed is > 737.5 mm/s for any value of laser power < 178 W (Figure 17a). The minimum wear volume would also be obtained at scan speed > 737.5 mm/s irrespective of the hatch spacing (Figure 17b).

(a) (b)

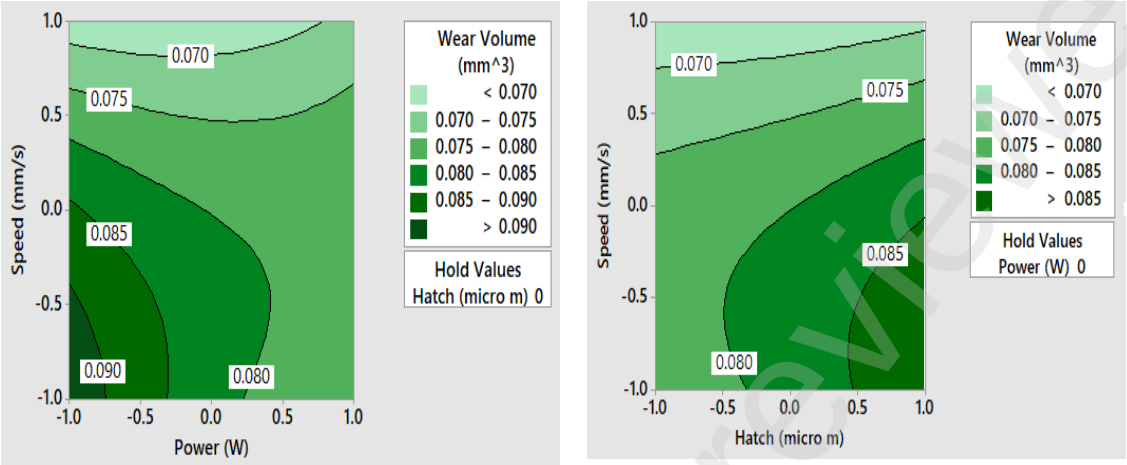

Figure 17 (a) Contour plot of the influence of scan speed and laser power on wear volume (b) Contour plot of the influence of scan speed and hatch spacing on wear volume

4.3 ANN Model

4.3.1 Analysis and validation of the ANN model

The performance of the ANN model was measured with the correlation coefficient R^2 and mean square error (MSE). The regression plot for training R value of 0.97833, validation R value of 0.99834, testing R value of 0.9997 and overall network prediction R value of 0.98472 against the experimental results are presented in Figure 18. The overall R value of 0.98472 indicates that the model accurately predicts the responses.

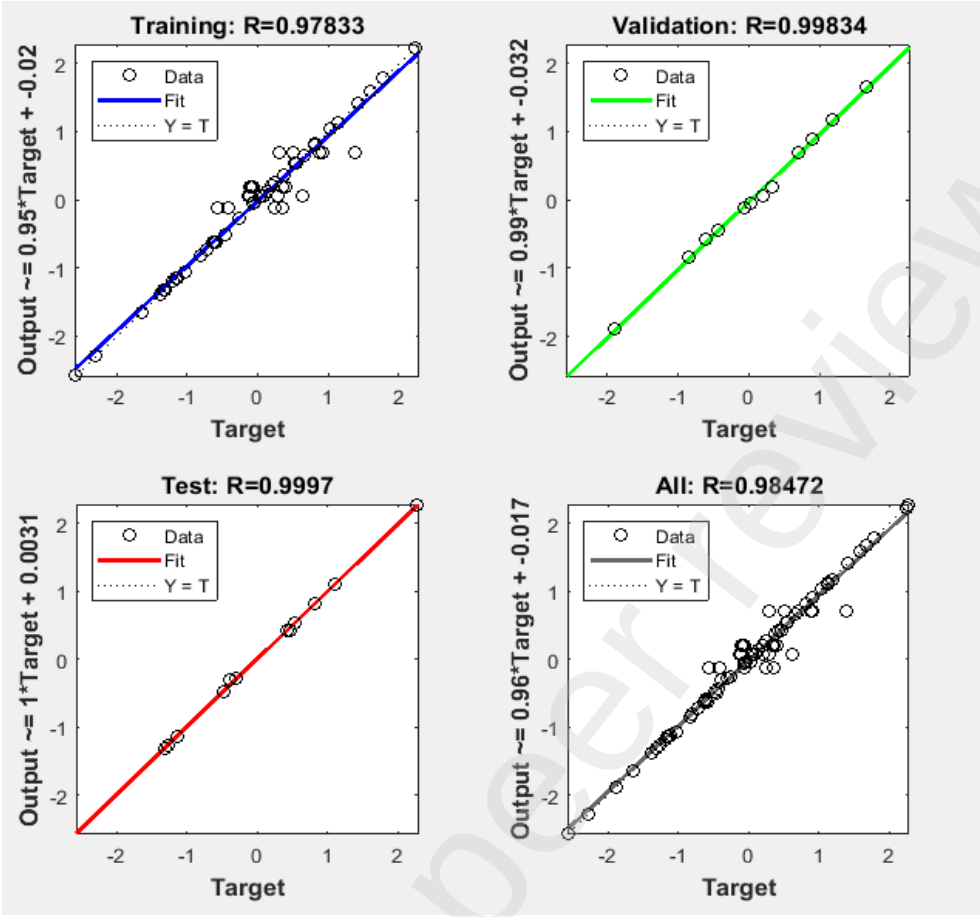

Figure 18 Regression plots of the ANN model

The training performance of the model is presented by the MSE variation graph in Figure 19. Similar characteristic of the test and validation graphs indicates that there was no significant over-fitting. The training was terminated in 9 epochs, the best performance was 0.00479 at epoch 3.

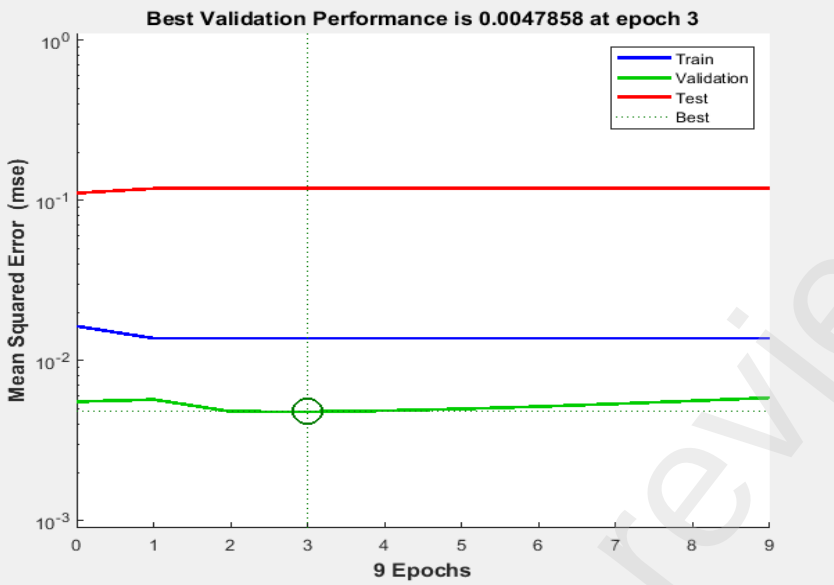

Figure 19 Model training, validation and testing MSE performance

5.0 Comparison of response surface modelling and artificial neural network model's results with experimental outcomes

Comparison of the experimental results with the ANN and RSM predicted responses is shown in Table 5. The ANN model is more accurate than the RSM model as its predicted results are closer to the experimental results as shown in Figure 20, Figure 21, Figure 22 and Figure 23. The prediction accuracy of the ANN and RSM models was also compared based on their coefficient of determination R^2. The ANN model with coefficient of determination R^2 value of 0.97 was more accurate than the RSM models with coefficient of determination R^2 values of 0.92 for porosity and 0.94 for microhardness, martensite phase composition and wear volume. The higher predicting ability of the ANN model could be due to its capability to generalize nonlinear systems. However, building RSM models may consume less time since it performs single step second order calculations compared to ANN that consumes more computational time to create and train because of the many associated iterative calculations.

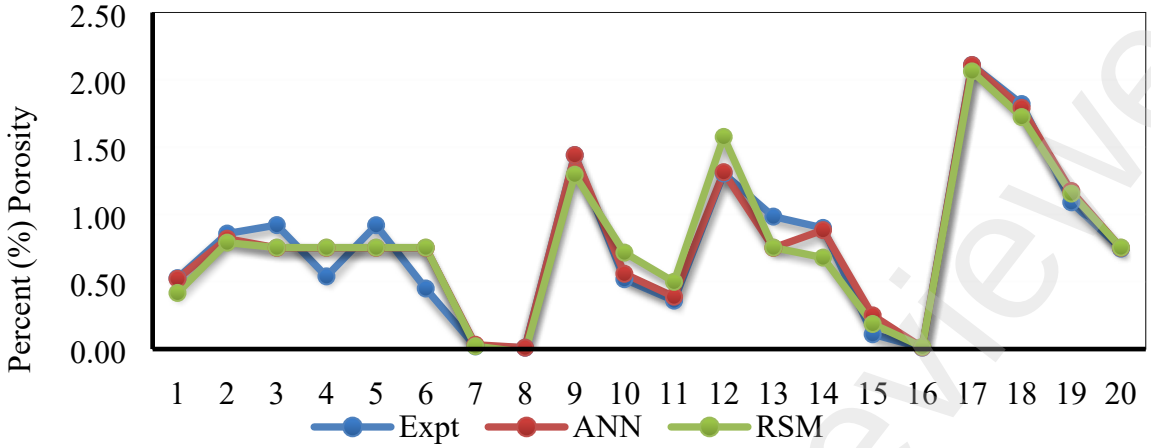

Figure 20. Comparison of experimental outcomes with ANN and RSM models results on porosity

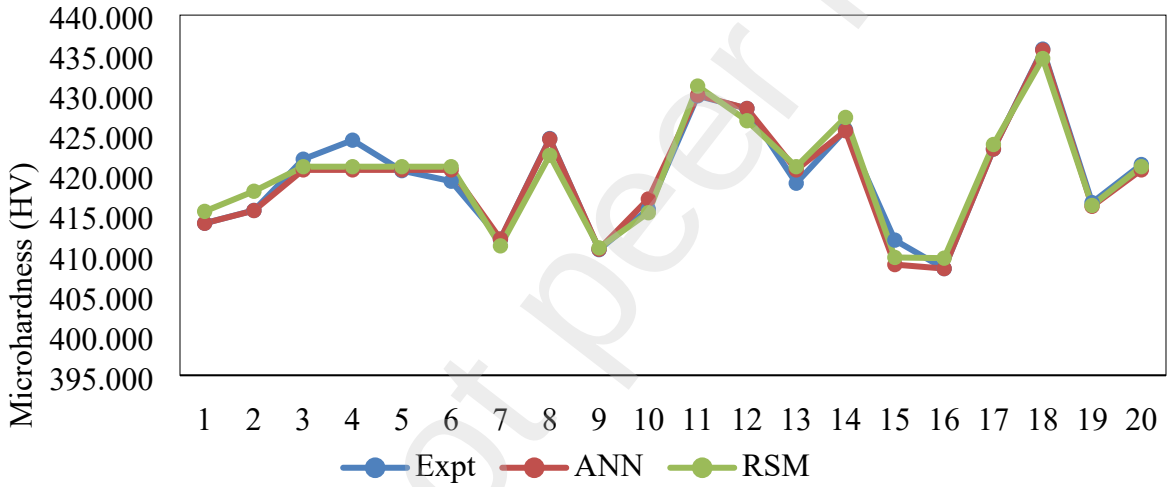

Figure 21 Comparison of experimental outcomes with ANN and RSM models results on microhardness

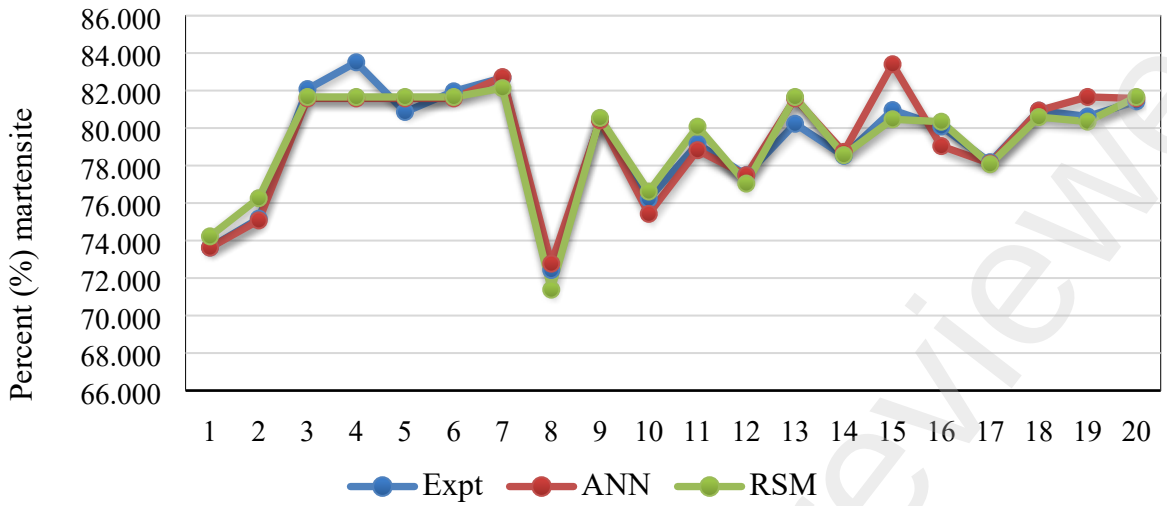

Figure 22 Comparison of experimental outcomes with ANN and RSM models results on martensite phase composition

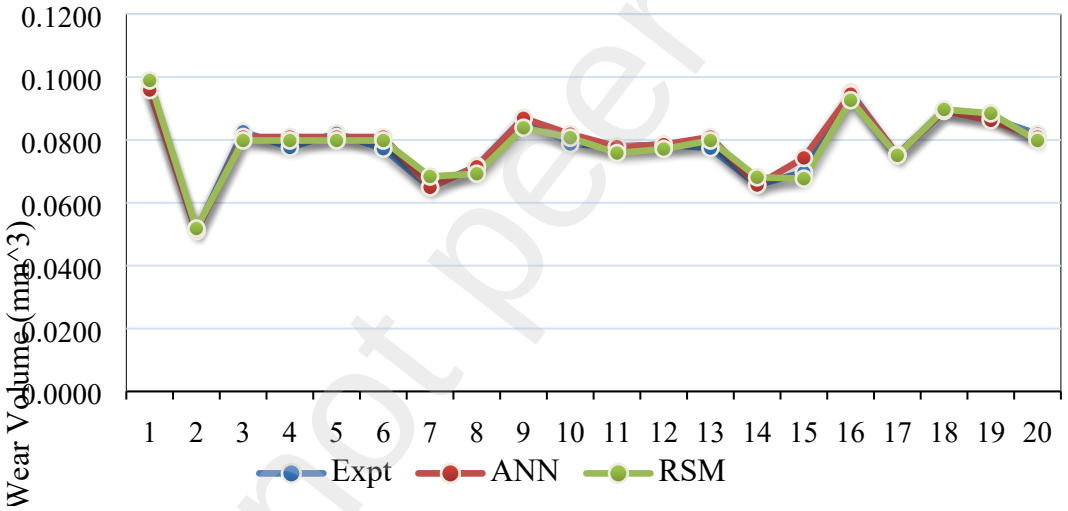

Figure 23. Comparison of experimental outcomes with ANN and RSM models results on wear volume

6.0 Optimisation and validation via RSM and ANN

The optimum LPBF processing parameters for minimum wear volume, minimum porosity, optimum microhardness and amount martensite phase composition were obtained by applying the developed RSM model. The RSM desirability function approach to multiple responses optimisation technique was used to optimise the responses. The desirability function approach transforms multiple response data to a single response by performing mathematical transformations [38]. Equation 12 describes the mathematical relationship of the desirability function (D(Y)) with responses [39].

$$\max D(Y) = (d_1(y_1)^{k_1} \times d_2(y_2)^{k_2} \times \ldots \times d_n(y_n)^{k_n})^{\frac{1}{\sum_i k_i}} \quad (12)$$

Where y_i is the determined value of response *i*, k_i is the relative importance of response *i* relative to other responses, $d_i(y_i)$ is the converted desirability value of *i'th* response.

The optimisation goal was to achieve minimum wear volume and porosity while maintaining maximum microhardness and amount of martensite phase composition. It was noted from this study that desired laser power for improving wear resistance also improves the amount of martensite and microhardness however it tends to contradict that of porosity. The preferred scan speed for improving wear resistance improves microhardness however it tends to oppose that of porosity and amount of martensite phase composition. The desired hatch spacing for enhancing wear resistance also improves porosity and microhardness however it tends to contradict that of the amount of martensite phase composition. Hence the need to balance the processing parameters to obtain low wear volume and porosity whilst maintaining preferred amount of martensite phase composition and microhardness. More weight was assigned to minimum wear volume and porosity. Solution 1 (Where p is the laser power, *v* is the scanning speed, *d* is hatch spacing and *t* is layer thickness.

) with desirable function 0.847 was the selected optimum operating parameters. The LPBF processing parameters are laser power = 165 W, scan speed = 784 mm/s and hatch spacing = 91 µm. The process volumetric energy density (VED) = 77 J/mm³ (Equation 13). The RSM predicted quality properties under these operating conditions are porosity = 0.01 %, microhardness = 411 HV, amount of martensite = 77.2 % and wear volume = 0.051 mm³.

$$VED = \frac{P}{v \times d \times t} \quad (13)$$

Where *p* is the laser power, *v* is the scanning speed, *d* is hatch spacing and *t* is layer thickness.

Table 10

RSM process optimisation

Solution	Power (W)	Scan speed (mm/s)	Hatch spacing (µm)	Porosity (%)	Microhardness (HV)	Martensite (%)	Wear Volume (mm^3)	Desirability	Selected
1	**165.074**	**784.000**	**91.012**	**0.010**	**411.055**	**77.186**	**0.051**	**0.847**	**X**
2	186.818	623.649	86.600	0.119	427.848	73.964	0.050	0.740	
3	186.818	619.922	86.600	0.186	428.121	73.988	0.048	0.660	
4	186.191	625.220	86.600	0.180	428.769	74.266	0.051	0.656	
5	186.818	616.906	86.600	0.242	428.346	78.209	0.047	0.598	
6	186.818	616.121	86.600	0.257	428.405	73.992	0.047	0.582	
7	158.352	784.000	103.400	0.373	409.019	78.209	0.047	0.420	

6.1 Validation by experiments

The developed ANN model was used to validate the RSM optimum parameters of the selected solution 1 in

$$(\text{maxDY}) = (d_1(y_1)^{k_1} \times d_2(y_2)^{k_2} \times \ldots \times d_n(y_n)^{k_n})^{\frac{1}{\sum_i k_i}} \quad (12)$$

Where y_i is the determined value of response *i*, k_i is the relative importance of response *i* relative to other responses, $d_i(y_i)$ is the converted desirability value of *i'th* response.

The optimisation goal was to achieve minimum wear volume and porosity while maintaining maximum microhardness and amount of martensite phase composition. It was noted from this study that desired laser power for improving wear resistance also improves the amount of martensite and microhardness however it tends to contradict that of porosity. The preferred scan speed for improving wear resistance improves microhardness however it tends to oppose that of

porosity and amount of martensite phase composition. The desired hatch spacing for enhancing wear resistance also improves porosity and microhardness however it tends to contradict that of the amount of martensite phase composition. Hence the need to balance the processing parameters to obtain low wear volume and porosity whilst maintaining preferred amount of martensite phase composition and microhardness. More weight was assigned to minimum wear volume and porosity. Solution 1 (Where p is the laser power, *v* is the scanning speed, *d* is hatch spacing and *t* is layer thickness.

) with desirable function 0.847 was the selected optimum operating parameters. The LPBF processing parameters are laser power = 165 W, scan speed = 784 mm/s and hatch spacing = 91 µm. The process volumetric energy density (VED) = 77 J/mm³ (Equation 13). The RSM predicted quality properties under these operating conditions are porosity = 0.01 %, microhardness = 411 HV, amount of martensite = 77.2 % and wear volume = 0.051 mm³.

$$VED = \frac{P}{v \times d \times t} \tag{13}$$

Where *p* is the laser power, *v* is the scanning speed, *d* is hatch spacing and *t* is layer thickness.

. The ANN results in Table 11 were consistent with the RSM data, the minimum percentage error was 0.00 % on wear volume, 1.405 % on amount of martensite, 2.573 % on microhardness and the maximum percentage is 20.00% on porosity.

Table 11
Validation of the RSM optimized parameters by ANN

	Porosity (%)	Microhardness (HV)	Martensite (%)	Wear Volume (mm³)
RSM Predicted	0.010	411.06	77.19	0.051

ANN Predicted	0.012	421.63	78.51	0.051
Error (%)	20.000	2.57	1.71	0.000

Validation experiments were carried out to confirm the optimum process parameters established by RSM and ANN. Results from the confirmatory experiments were consistent with the RSM and ANN predictions (Table 12). The ANN model predictions were more accurate than the RSM model as its predicted results were closer to the experimental results as shown Table 12.

Table 12
Validation of RSM and ANN predicted by confirmatory experiment results

	Porosity (%)	**Microhardness (HV)**	**Martensite (%)**	**Wear Volume (mm^3)**
Validation Experiments Results	0.21	353.6	80.4	0.053
RSM Predicted	0.010	411.1	77.2	0.051
Error (%)	95.24	-16.26	+3.98	+3.77
Validation Experiments Results	0.21	353.6	80.4	0.053
ANN Predicted	0.012	421.6	78.5	0.051
Error (%)	94.29	-19.23	+2.36	+3.77

7.0 Conclusions

A hybrid of ANN and RSM optimization technique was applied in this study to optimise microstructural and mechanical properties of LPBF manufactured maraging steel 1.2709 parts. Analysis of variance (ANOVA) indicated that the RSM models are suitable for predicting microstructural and mechanical properties of LPBF manufactured maraging steel. The ANOVA indicated that all three LPBF processing parameters (laser power, scanning speed and hatch spacing) have significant influence on the microstructural characteristics (porosity, microhardness and martensite phase) and wear resistance of manufactured maraging steel samples. The effects of individual and combined processing parameters were described by main effects and contour plots respectively. For example, the wear volume decreased to the minimum when power was increased until a value of laser power (178 W) was reached. The wear volume was observed to be increasing

when the power value exceeded 178 W. The main effects plot also described the relationship of microstructural properties with wear volume.

Performance analysis of the configured and trained ANN model with regression coefficient (R^2) and root mean squared error (RMSE) indicated that the model can successfully predict the optimum microstructural and mechanical properties. RSM and ANN were compared using the regression coefficient (R^2). The ANN model had a better predicting ability with coefficient of determination R^2 value of 0.97 compared to the RSM models with coefficient of determination R^2 values of 0.92 and 0.94. The results of the ANN and RSM models were compared with experimental results. Both models have a high tracking ability, however, ANN had better prediction accuracy than RSM.

The developed RSM model was applied to determine the optimum LPBF processing parameters and the results were validated by an ANN model. The most desirable optimum LPBF processing parameters for the specific machine and material were: laser power = 165 W, scan speed = 784 mm/s and hatch spacing = 91 μm with a desirable function of 0.847. The RSM predicted quality properties under these operating conditions are: porosity = 0.010 percent, microhardness = 411 HV, amount of martensite = 77.2 percent and wear volume = 0.051 mm^3. The RSM and ANN results are in good agreement with the error range of 0.00 to 20 %.

The RSM and ANN model predictions were consistent with confirmatory experiment results. The developed RSM and ANN models are suitable for predicting microstructural and mechanical properties of LPBF manufactured maraging steel.

Acknowledgements

This research is supported by the Botswana International University of Science and Technology (BIUST) Research Initiation Fund under Grant no S00195 and the Council for Scientific and Industrial Research (CSIR) through the African Laser Centre (ALC) under Grant no HLHA21X task ALC-R006.

References

[1] B. Vandenbroucke and J.-P. Kruth, "Selective Laser Melting of Biocompatible Metals for Rapid," *Rapid Prototyp. J.*, vol. 13, no. 4, pp. 148–159, 2007.

[2] C. Klahn, B. Leutenecker, and M. Meboldt, "Design Strategies for the Process of Additive Manufacturing," *Procedia CIRP*, vol. 36, pp. 230–235, 2015, doi: 10.1016/j.procir.2015.01.082.

[3] X. Qi, G. Chen, Y. Li, X. Cheng, and C. Li, "Applying Neural-Network-Based Machine Learning to Additive Manufacturing : Current Applications , Challenges , and Future Perspectives," *Engineering*, vol. 5, no. 4, pp. 721–729, 2019, doi: 10.1016/j.eng.2019.04.012.

[4] P. K. Gokuldoss, S. Kolla, and J. Eckert, 'Additive manufacturing processes: Selective laser melting, electron beam melting and binder jetting-selection guidelines', *Materials*. MDPI AG, 2017, https://doi.org/10.3390/ma10060672.

[5] E. O. Olakanmi, "Journal of Materials Processing Technology Selective laser sintering / melting (SLS / SLM) of pure Al , Al – Mg , and Al – Si powders : Effect of processing conditions and powder properties," *J. Mater. Process. Tech.*, vol. 213, no. 8, pp. 1387–1405, 2013, doi: 10.1016/j.jmatprotec.2013.03.009.

[6] Y. Bai, Y. Yang, D. Wang, and M. Zhang, "Influence mechanism of parameters process and mechanical properties evolution mechanism of maraging steel 300 by selective laser melting," *Mater. Sci. Eng. A*, vol. 703, no. July 2019, pp. 116–123, 2017, doi: 10.1016/j.msea.2017.06.033.

[7] E. Yasa, K. Kempen, J. P. Kruth, L. Thijs, and J. Van Humbeeck, "Microstructure and Mechanical Properties of Maraging Steel 300 After Selective Laser Melting," In *21st Annual International Solid Freeform Fabrication Symposium - An Additive Manufacturing Conference, SFF 2010* pp. 383–396, 2010.

[8] S. Mutua, James, NaKata and Z. Onda, Tetsuhiko and Chen, "Optimization of selective laser melting parameters and in fl uence of post heat treatment on microstructure and mechanical properties of maraging steel," *Mater. Des.*, vol. 139, pp. 486–497, 2018, doi: 10.1016/j.matdes.2017.11.042.

[9] P. Hanzl, M. Zetek, T. Bakša, and T. Kroupa, "The Influence of Processing Parameters on the Mechanical Properties of SLM Parts," *Procedia Eng.*, vol. 100, pp. 1405–1413, 2015, doi: 10.1016/j.proeng.2015.01.510.

[10] Z. Guo and W. Sha, "Modelling the correlation between processing parameters and properties of maraging steels using artificial neural network," *Computational Materials Science*, *29*(1), pp. 12–28, 2004, doi: 10.1016/S0927-0256(03)00092-2.

[11] B. Podgornik, M. Šinko, and M. Godec, "Dependence of the wear resistance of additive-manufactured maraging steel on the build direction and heat treatment," *Addit. Manuf.*, vol. 46, no. January, 2021, doi: 10.1016/j.addma.2021.102123.

[12] T. B. Sirin and Y. Kaynak, "Surface Integrity and Wear Resistance of Maraging Steel Produced by Additive Manufacturing Direct Metal Laser Sintering," *J. Adv. Manuf. Eng.*, no. October, 2020.

[13] G. M. S. Ahmed, I. A. Badruddin, V. Tirth, A. Algahtani, and M. A. Ali, "Wear resistance of maraging steel developed by direct metal laser sintering," *Mater. Express*, vol. 10, no. 7, pp. 1079–1090, 2020, doi: 10.1166/mex.2020.1715.

[14] F. Cajner, D. Landek, and V. Leskovšek, "Surface modifications of maraging steels used in the manufacture of moulds and dies," *Mater. Tehnol.*, vol. 44, no. 1, pp. 101–107, 2010.

[15] F. Karimi, S. Rafiee, A. Taheri-Garavand, and M. Karimi, "Optimization of an air drying process for Artemisia absinthium leaves using response surface and artificial neural network models," *J. Taiwan Inst. Chem. Eng.*, vol. 43, no. 1, pp. 29–39, 2012, doi: 10.1016/j.jtice.2011.04.005.

[16] B. Rezaei, M. Askari, A. Mousavi Shoushtari, M. Ghani, and A. Haji, "Application of response surface methodology (RSM) and artificial neural network (ANN) in diameter optimization of thermo regulating nanofibers," *5th TEXTEH Int. Conf.*, no. October, 2012.

[17] B. Bachy and J. Franke, "Modeling and optimization of laser direct structuring process using artificial neural network and response surface methodology," *Int. J. Ind. Eng. Comput.*, vol. 6, no. 4, pp. 553–564, 2015, doi: 10.5267/j.ijiec.2015.4.003.

[18] S. Chamoli, "ANN and RSM approach for modeling and optimization of designing parameters for a V down perforated baffle roughened rectangular channel," *Alexandria Eng. J.*, vol. 54, no. 3, pp. 429–446, 2015, doi: 10.1016/j.aej.2015.03.018.

[19] S. Sada, "Modeling Performance of Response Surface Methodology and Artificial Neural Network DOI : https://dx.doi.org/10.4314/jasem.v22i6.6," 2018.

[20] N. Syuhadah *et al.*, "Artificial Neural Networks (ANNs) and Response Surface Methodology (RSM) Approach for Modelling the Optimization of Chromium (VI) Reduction by Newly Isolated Acinetobacter radioresistens Strain NS-MIE from Agricultural Soil," *BioMed Research International*, *2019*. https://doi.org/10.1155/2019/5785387..

[21] L. A. Dobrzański, M. Kowalski, and J. Madejski, "Methodology of the mechanical properties prediction for the metallurgical products from the engineering steels using the Artificial Intelligence methods," *J. Mater. Process. Technol.*, vol. 164–165, pp. 1500–1509, 2005, doi: 10.1016/j.jmatprotec.2005.02.194.

[22] Andrej Krenker, J. Bešter, and A. Kos, "Introduction to the Artificial Neural Networks, In: Suzuki K (ed), Artificial Neural Networks: Methodological Advances and Biomedical Applications," *InTech*, pp. 1–18, 2011, doi: 10.5772/15751.

[23] C. M. A.-C. Raymond H. Myers, Douglas C. Montgomery, *Response surface methodology : process and product optimization using designed experiments. - - 3rd ed.*, 3rd ed. John Wiley & Sons, Inc., Hoboken, New Jersey Published, 2009.

[24] K. M. Carley, "Response Surface Methodology," *CASOS - Center for Computational Analysis of Social and Organizational Systems* CMU-ISRI-04-136 2014 https://www.researchgate.net/publication/235080757.

[25] H. N. Koivo, "Neural Networks : Basics using MATLAB Neural Network Toolbox," *Neural Networks*, pp. 1–59, 2008.

[26] M. Gopal, "Network architectures," in *Applied Machine Learning*, New York, Chicago, San Francisco, Athens, London, Madrid, Mexico City, Milan, New Delhi, Singapore, Sydney, Toronto: McGraw-Hill Education, 2019.

[27] L. Mugwagwa, I. Yadroitsev, and S. Matope, "Effect of Process Parameters on Residual Stresses , Distortions , and Porosity in Selective Laser Melting of Maraging Steel 300 Effect of Process Parameters on Residual Stresses , Distortions , and Porosity in Selective Laser

Melting of Maraging Steel 300," *Metals*, *9*(10), 2019, doi: 10.3390/met9101042.

[28] M. Terner, T. Ricordel, J.-H. Cho, and J.-S. Lee, "The Response Surface Methodology for Optimizing the Process Parameters of Selective Laser Melting," *Journal of Welding and Joining*, *37*(1), 27–39 , 2019 https://doi.org/10.5781/jwj.2019.37.1.4.

[29] J. Qu and J. J. Truhan, "An efficient method for accurately determining wear volumes of sliders with non-flat wear scars and compound curvatures," *Wear*, vol. 261, no. 7–8, pp. 848–855, 2006, doi: 10.1016/j.wear.2006.01.009.

[30] L. Thijs, F. Verhaeghe, T. Craeghs, J. Van Humbeeck, and J. P. Kruth, "A study of the microstructural evolution during selective laser melting of Ti-6Al-4V," *Acta Mater.*, vol. 58, no. 9, pp. 3303–3312, 2010, doi: 10.1016/j.actamat.2010.02.004.

[31] K. Kempen, E. Yasa, L. Thijs, J. P. Kruth, and J. Van Humbeek, "Microstructure and mechanical properties of Selective Laser Melted 18Ni-300 steel," *Physics Procedia* vol. 12, pp. 255–263, 2011, doi: 10.1016/j.phpro.2011.03.033.

[32] R. Casati, J. N. Lemke, A. Tuissi, and M. Vedani, "Aging Behaviour and Mechanical Performance of 18-Ni 300 Steel Processed by Selective Laser Melting," *Metals*, *6*(9), 2016, doi: 10.3390/met6090218.

[33] E. I. Galindo-Nava, W. M. Rainforth, and P. E. J. Rivera-Díaz-del-Castillo, "Predicting microstructure and strength of maraging steels: Elemental optimisation," *Acta Mater.*, vol. 117, pp. 270–285, 2016, doi: 10.1016/j.actamat.2016.07.020.

[34] Z. Yusoff and S. B. Jamaludin, "Tribology and Development of Wear Theory: Review and Discussion," *Int. J. Curr. Res. Rev.*, vol. 3, no. February 2011, pp. 13–26, 2011.

[35] C. Tan, K. Zhou, W. Ma, P. Zhang, M. Liu, and T. Kuang, "Microstructural evolution , nanoprecipitation behavior and mechanical properties of selective laser melted high-performance grade 300 maraging steel," *Mater. Des.*, vol. 134, pp. 23–34, 2017, doi: 10.1016/j.matdes.2017.08.026.

[36] W. Wu *et al.*, "Microstructure and mechanical properties of maraging 18Ni-300 steel obtained by powder bed based selective laser melting process," *Rapid Prototyp. J.*, vol. 26, no. 8, pp. 1379–1387, 2020, doi: 10.1108/RPJ-08-2018-0189.

[37] D. Do, "The effect of laser energy input on the microstructure , physical and mechanical properties of Ti-6Al-4V alloys by selective laser melting," *Virtual and Physical Prototyping*, *11*(1), 41–47 no. May, 2018, doi: 10.1080/17452759.2016.1142215.

[38] E. Del Castillo, D. C. Montgomery, and D. R. McCarville, "Modified desirability functions for multiple response optimization," *J. Qual. Technol.*, vol. 28, no. 3, pp. 337–345, 1996, doi: 10.1080/00224065.1996.11979684.

[39] H. Akçay and A. S. Anagün, "Multi response optimization application on a manufacturing factory," *Math. Comput. Appl.*, vol. 18, no. 3, pp. 531–538, 2013, doi: 10.3390/mca18030531.